Journal of Earthquake Engineering

ISSN: 1363-2469 (Print) 1559-808X (Online) Journal homepage: http://www.tandfonline.com/loi/ueqe20

Modeling Techniques for the Seismic Assessment of the Existing Italian RC Frame Structures

Gerard J O'Reilly & Timothy J Sullivan

To cite this article: Gerard J O'Reilly & Timothy J Sullivan (2017): Modeling Techniques for the Seismic Assessment of the Existing Italian RC Frame Structures, Journal of Earthquake Engineering, DOI: 10.1080/13632469.2017.1360224

To link to this article: http://dx.doi.org/10.1080/13632469.2017.1360224

Accepted author version posted online: 17 Aug 2017.
Published online: 17 Aug 2017.

JOURNAL OF EARTHQUAKE ENGINEERING
https://doi.org/10.1080/13632469.2017.1360224

Taylor & Francis
Taylor & Francis Group

Modeling Techniques for the Seismic Assessment of the Existing Italian RC Frame Structures

Gerard J O'Reilly[a] and Timothy J Sullivan[b]

[a]Scuola Universitaria Superiore IUSS Pavia, Pavia Italy; [b]Department of Civil Engineering and Natural Resources, University of Canterbury, Christchurch, New Zealand

ABSTRACT

A numerical modeling approach to capture the behavior of the various elements of older reinforced concrete (RC) frames in Italy is developed. It uses available experimental data to calibrate an approach that accounts for the strength and stiffness degradation of the members. The effects of smooth reinforcing bars on the hysteretic behavior and the overall flexural deformation capacity of members are considered. The means of accounting for strength and stiffness degradation in exterior beam-column joints is also studied and calibrated to the available experimental test data. The performance of the proposed modeling approach for older RC frames in Italy is then appraised by comparing the predictions with experimental results for two different three-story frame specimens tested both statically and pseudo-dynamically. The benefits of using the new modeling techniques for the existing RC frame structures instead of more traditional approaches is also highlighted.

ARTICLE HISTORY
Received 8 February 2017
Accepted 17 July 2017

KEYWORDS
Modeling; Assessment; Non-Ductile; Gravity Load Design; RC Frames

1. Introduction

The behavior of the existing RC structures in Italy and across the Mediterranean area has been the focus of much research over the past number of years. In Italy, prior to the introduction of seismic design provisions in the 1970s, structural design was largely based on the Royal Decree [Regio Decreto, 1939] published in 1939. This document provided a basis for structural design in Italy for the best part of 30 years, during which a large number of RC frame structures were built in the reconstruction after World War II. Allowable stress values were used in design and smooth reinforcing bars anchored with end-hooks in the beam-column joints were also quite common, with the beam-column joint region typically being void of transverse reinforcement. Such frames will be referred to as gravity load designed (GLD) frames herein, recognizing that they were designed with a complete lack of seismic design provisions. Survey data [ISTAT, 2011] indicates that over 30% of the existing RC frame building stock in Italy comprises of GLD frames, which have been recently shown by Del Gaudio et al. [2016] to be quite vulnerable to damage due to seismic loading following the 2009 L'Aquila event.

Seismic assessment of the existing structures aims to identify the expected damage mechanism in a structure and evaluate the potential implications of this on the overall

CONTACT Gerard J O'Reilly gerard.oreilly@iusspavia.it Scuola Universitaria Superiore IUSS Pavia, Palazzo del Broletto, Piazza della Vittoria 15, Pavia 27100 Italy.

Color versions of one or more of the figures in the article can be found online at www.tandfonline.com/UEQE.

building performance. Appropriate numerical modeling tools are required so that the response of the various components vulnerable to damage can be adequately assessed via numerical analyses. Unfortunately, guidelines available for the analysis of modern ductile RC frame structures cannot be considered applicable in the case of the existing GLD RC frames in Italy. A number of guidelines do exist for the non-linear modeling and analysis of GLD RC frames in Italy [Calvi, Magenes, and Pampanin, 2002a; Landi, Tardini, and Diotallevi, 2016; Metelli, Messali, Beschi, and Riva, 2015; Pampanin, Magenes, and Carr, 2003] but these do not appear to account for strength and stiffness degradation in the various components, which are imperative for collapse and risk assessment studies on the existing building stock. As such, this paper aims to bridge the gap for the comprehensive structural analysis of GLD frames in Italy by amalgamating available experimental data to then calibrate and validate numerical models that represent the behavior of the various elements, such as beam-column frame elements and joints. The results of two different three story specimens tested pseudo-statically and pseudo-dynamically are then used to highlight the benefits offered by the numerical modeling approach proposed here. It is noted that this article focuses on modeling the response of the RC frame alone and the interaction with masonry infill, common in Italian construction, is not covered in detail. However, the approach outlined here can be adapted such that the shear failure in RC columns due to infill interaction can be represented by adopting an equivalent diagonal truss layout as suggested in Crisafulli, Carr, and Park [2000] with the hysteretic backbone computed as per Sassun, Sullivan, Morandi, and Cardone [2015]. A further description of this implementation can be found in O'Reilly [2016].

2. Observed Behavior of GLD Frames

2.1. *Past Performance During Earthquakes*

Among the different damage mechanisms reported from recent earthquake events, non-ductile response of column members was frequently encountered [Augenti and Parisi, 2010; Ricci, De Luca, and Verderame, 2011; Salvatore, Caprilli, and Barberi, 2009; Verderame, Iervolino, and Ricci, 2009]. Many existing buildings in Italy possess column members that are susceptible to shear failure. This results as they were principally sized to meet axial load capacity requirements and contain little transverse shear reinforcement, which were closed with 90° hooks. One of the more infamous cases of shear failure in RC frame structures during past seismic events in Italy occurred at the San Salvatore Hospital in L'Aquila. The shear failure of three columns (one of which is shown in Fig. 1) along with the out-of-plane failure of masonry partition walls resulted in the evacuation of the hospital, which would have been otherwise critical in providing medical aid following the earthquake. While Augenti and Parisi [2010] noted that the failure of the columns may have been due to the relatively large vertical excitation component recorded during the L'Aquila main shock, a lack of effective transverse shear reinforcement and poor confinement was evident and the mechanism appeared typical of a shear failure.

In addition to detailing members to avoid brittle shear failure, modern design codes enforce what is commonly referred to as "capacity design", whereby a strength hierarchy is maintained such that a ductile beam-sway mechanism develops [Park and Paulay, 1975]. Since older design codes did not enforce these capacity design requirements, many

Figure 1. Column shear failure at San Salvatore hospital in L'Aquila [Augenti and Parisi, 2010].

buildings possess weak storys that are vulnerable to developing a non-ductile column sway collapse mechanism. An example of this is illustrated in Fig. 2, where a soft story mechanism formed in the second story of a residential structure in L'Aquila. Augenti and Parisi [2010] also reported that the story completely collapsed in the building resulting in many fatalities.

Furthermore, the plastic hinging that forms at the column ends during a soft story mechanism also tends to be fundamentally different. Experimental testing [Di Ludovico, Verderame, Prota, Manfredi, and Cosenza, 2013; Melo, Varum, and Rossetto, 2015; Verderame, Fabbrocino, and Manfredi, 2008b] has highlighted that use of smooth bars in RC frame members tends to result in fewer but wider flexural cracks along the plastic hinge zone, whereas an equivalent specimen detailed with deformed bars tends to form smaller cracks and distribute the inelasticity along the plastic hinge zone much better. Figure 3 illustrates this aspect that is also supported by different experimental test campaigns like Melo, Varum, and Rossetto [2015], for example.

In addition to the poor performance of RC frame members, significant damage to beam-column joints has been observed during past earthquakes in Italy [Bursi, Dusatti, and Pucinotti, 2009; Celano, Cimmino, Coppola, Magliulo, and Salzano, 2016; Verderame, Iervolino, and Ricci, 2009]. Figure 4 shows some examples of beam-column joint failure from the L'Aquila event in 2009, where the concrete is seen to crack, spall and crush under the

Figure 2. Second story collapse of a residential RC frame building in L'Aquila [Augenti and Parisi, 2010].

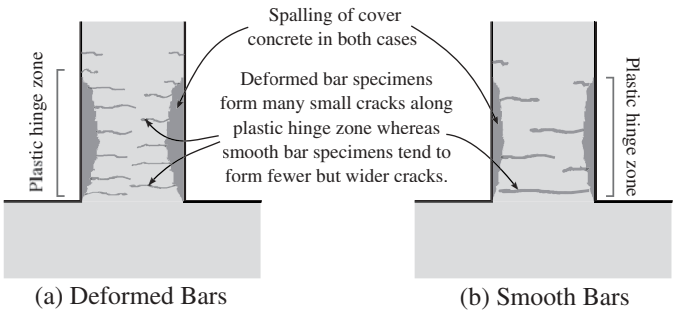

Figure 3. Illustration of differences in plastic hinging of members with deformed and smooth bars, where smooth bar specimens tend to form fewer but wider flexural cracks in plastic hinge zone compared to their deformed bar counterparts, as demonstrated experimentally by Melo, Varum, and Rossetto [2015], for example.

(a) Buckling of joint reinforcement.

(b) Diagonal cracking of the beam-column joint.

(c) Loss of cover concrete and severe degradation of the concrete within the joint.

(d) Loss of cover concrete and damage to the joint.

Figure 4. Typical beam-column joint damage observed in L'Aquila, 2009 and Rieti, 2016 (Images (a) and (b) are adopted from Verderame, Iervolino, and Ricci [2009], (c) is adopted from Bursi, Dusatti, and Pucinotti [2009] and (d) is adopted from Celano, Cimmino, Coppola, Magliulo, and Salzano [2016]).

seismic demand due to a lack of transverse shear reinforcement in the joint region. Fig. 4(b) shows a typical example of this type of failure mechanism, where the principle tensile stress developed in the joint results in a diagonal crack forming, which is illustrated further in Fig. 5. In addition to this, the lack of transverse shear reinforcement in the joint can result in buckling of the longitudinal reinforcement (Fig. 4(a)) that may lead to a loss of shear as well as axial load carrying capacity of the joint.

2.2. *Experimental Testing*

2.2.1. *Beam-Column Members*

The behavior of beam-column members with smooth reinforcement and transverse shear reinforcement closed with 90° hooks differs to those with deformed bars and stirrups closed at 135° due to the poor bond strength between the bar and the concrete paste

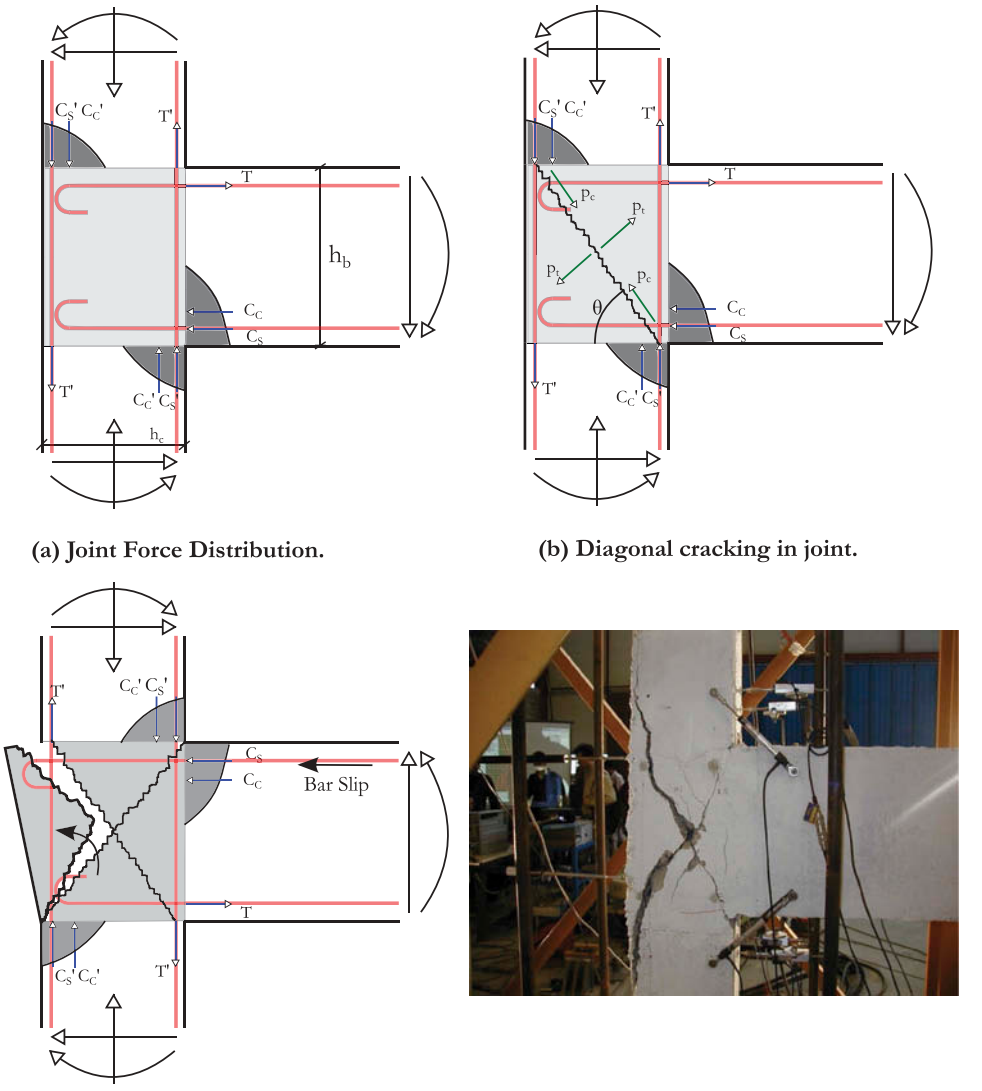

(a) Joint Force Distribution.

(b) Diagonal cracking in joint.

(c) Diagonal cracking on load reversal and ejection of concrete wedge.

(d) Experimental observation from Pampanin et al. [2002].

Figure 5. Diagonal cracking of joint and formation of "concrete wedge" mechanism in specimen tested by Pampanin, Calvi, and Moratti [2002].

resulting in a more pinched hysteretic behavior. A number of experimental test campaigns have been conducted on beam-column members with smooth bars to establish their hysteretic behavior and are listed in Table 1, where ν refers to axial load ratio, ρ and ρ' represent the tensile and compressive reinforcement ratios, respectively, and ρ_V represents the transverse shear reinforcement ratio. For example, Verderame et al. [2008a; 2008b] conducted both monotonic and cyclic testing on a number of RC beam-columns with smooth reinforcing bars and bar lapping just above the column base. In general, they were

Table 1. Experimental database of 23 test specimens collected from the literature for beam-column members with smooth bars and lapping typical of pre-1970 Italian RC frame construction.

#	Reference	ID	b x h [cm]	ν	ρ	ρ′	ρ_v	Loading	Lapping
1	Verderame et al. [2008b]	C-270A1	30x30	0.12	0.43%	0.43%	0.34%	Cyclic	40Ø
2	Verderame et al. [2008b]	C-270A2	30x30	0.12	0.43%	0.43%	0.34%	Cyclic	40Ø
3	Verderame et al. [2008b]	C-270B1	30x30	0.12	0.43%	0.43%	0.34%	Cyclic	Continuous
4	Verderame et al. [2008b]	C-540A1	30x30	0.24	0.43%	0.43%	0.34%	Cyclic	40Ø
5	Verderame et al. [2008b]	C-540B1	30x30	0.24	0.43%	0.43%	0.34%	Cyclic	Continuous
6	Verderame et al. [2008b]	C-540B2	30x30	0.24	0.43%	0.43%	0.34%	Cyclic	Continuous
7	Melo, Varum, and Rossetto [2015]	CPA-1	30x30	0.16	0.43%	0.43%	0.17%	Cyclic	Continuous
8	Melo, Varum, and Rossetto [2015]	CPA-3	30x30	0.19	0.43%	0.43%	0.17%	Cyclic	Continuous
9	Melo, Varum, and Rossetto [2015]	CPB	30x30	0.17	0.43%	0.43%	0.17%	Cyclic	30Ø
10	Melo, Varum, and Rossetto [2015]	CPC	30x30	0.20	0.57%	0.57%	0.17%	Cyclic	Continuous
11	Melo, Varum, and Rossetto [2015]	CPD	30x30	0.19	0.57%	0.57%	0.17%	Cyclic	30Ø
12	Melo, Varum, and Rossetto [2015]	CPE	30x40	0.14	0.31%	0.31%	0.17%	Cyclic	Continuous
13	Melo, Varum, and Rossetto [2015]	CPF	30x50	0.11	0.32%	0.32%	0.17%	Cyclic	Continuous
14	Verderame et al. [2008a]	M-270A1	30x30	0.12	0.43%	0.43%	0.34%	Monotonic	40Ø
15	Verderame et al. [2008a]	M-270A2	30x30	0.12	0.43%	0.43%	0.34%	Monotonic	40Ø
16	Verderame et al. [2008a]	M-270B1	30x30	0.12	0.43%	0.43%	0.34%	Monotonic	Continuous
17	Verderame et al. [2008a]	M-270B2	30x30	0.12	0.43%	0.43%	0.34%	Monotonic	Continuous
18	Verderame et al. [2008a]	M-540A1	30x30	0.24	0.43%	0.43%	0.34%	Monotonic	40Ø
19	Verderame et al. [2008a]	M-540B1	30x30	0.24	0.43%	0.43%	0.34%	Monotonic	Continuous
20	Di Ludovico et al. [2014]	S300P-m	30x30	0.20	0.43%	0.43%	0.22%	Monotonic	Continuous
21	Di Ludovico et al. [2014]	S300P-c	30x30	0.20	0.43%	0.43%	0.22%	Cyclic	Continuous
22	Di Ludovico et al. [2014]	R300p-c	50x30	0.10	0.43%	0.43%	0.13%	Cyclic	Continuous
23	Di Ludovico et al. [2014]	R500p-c	30x50	0.10	0.24%	0.24%	0.22%	Cyclic	Continuous

found to give satisfactory behavior in terms of their overall deformation capacity, although it was noted that this comes from a concentration in end-rotation along a few cracks resulting in a localized deformation as opposed to a larger spread in plasticity along the member plastic hinge zone that is more typical of members possessing deformed bars, as illustrated in Fig. 3. The overall hysteretic dissipation of the specimens is noticeably more pinched due to the presence of smooth bars than what is typically observed with members containing deformed bars. Melo, Varum, and Rossetto [2015], for example, concluded that the presence of smooth bars resulted in a reduction of energy dissipation and a more pinched hysteretic behavior, whereas columns with large cross-sections tended to suffer more pinching than smaller cross-sections. Verderame, Fabbrocino, and Manfredi [2008b] also compared the ultimate chord rotation capacity observed in the tests and the predicted capacity using the expression in Eurocode 8 [EN 1998-3:2005, 2005] that defines the ultimate chord rotation corresponding to a 20% loss in load carrying capacity. Modifications to the expression given in Eurocode 8 have been proposed with the intention of accounting for the lack of seismic detailing and the use of smooth bars. Examining this comparison by Verderame, Fabbrocino, and Manfredi [2008b], the expression in Eurocode 8 tends to underestimate the ultimate chord rotations of the members with smooth bars, especially in the case of columns with low axial load ratio. Subsequently, Verderame et al. [2010] conducted a review of the various parameters used by the Eurocode 8 expression to evaluate ultimate chord rotation capacity while accounting for old member detailing and bar lapping. Using experimental data, assessed and proposed a modification to the existing expressions provided by the 2009 edition of Eurocode 8 [EN 1998-3:2009, 2009] to account for the use of smooth bars with lapping as a result of more recent experimental test data. In terms of using smooth bars, experimental tests carried

out on similar specimens with both smooth and deformed bars by Di Ludovico, Verderame, Prota, Manfredi, and Cosenza [2013] showed an increase in the ultimate deformation capacity of RC beam-columns with smooth bars by about 40% when compared to the corresponding deformed bar specimens. This was noted as a result of the increased end rotation in the plastic hinge zone. This is contrary to the initial proposal within Eurocode 8, which initially looked to reduce the ultimate rotation capacity of the member due to the presence of smooth bars, whereas experimental evidence has shown the contrary. Melo, Varum, and Rossetto [2015] also more recently noted that spalling and buckling of the longitudinal reinforcement starts at an earlier stage in specimens with smooth bars and widely spaced stirrups closed at 90° compared to specimens with deformed bars and stirrups closed as 135°; however, the net effect on the deformation capacity is an increase due to the additional end rotation.

2.2.2. *Exterior Beam-Column Joints*

Pampanin, Calvi, and Moratti [2002] tested two sub-assemblages of exterior beam-column joints with end-hooks and smooth reinforcing bars typical of pre-1970 Italian construction. The performance of these joints was shown to be quite brittle, where diagonal cracking of the joint along with slippage of longitudinal bars led to concrete being spalled off, in what was termed the "concrete wedge" by Pampanin, Calvi, and Moratti [2002]. This resulted from insufficient joint transverse shear reinforcement leading to cracking of the joint concrete from excess loading, as illustrated in Fig. 5. In a similar study discussed later in Section 4.2, Calvi et al. [2002b] tested an RC frame with detailing typical of pre-1970s construction in Italy, where the damage sustained by the structure was concentrated in the exterior beam-column joints of the bottom two storys, with the "concrete wedge" behavior being observed. The result of this concrete wedge spalling on either end of the structure meant a shear hinge mechanism formed in the joints, which then spread the increased deformation of the joint over the two adjacent storys as opposed to a single story, which would have been the case had flexural hinging formed in the column members. Furthermore, Braga, Gigliotti, and Laterza [2009] and Akguzel [2011] tested exterior joints constructed to pre-1970 Italian detailing standards and their observations were as previously reported in Pampanin, Calvi, and Moratti [2002] with high pinching, low energy dissipation and the aforementioned wedge mechanism. In the specimen tested by Akguzel [2011], this formation of the wedge at around 3% drift resulted in the buckling of the column longitudinal bars in the joint, although no axial load readings were provided to establish the level of force required to cause the buckling of the column bars.

3. Numerical Modeling of GLD Frame Members

3.1. *Beam-Column Frame Members*

To model the behavior of GLD RC frame members, it is important to accurately represent the behavior of the beams and columns constructed with outdated practice; such as the use of smooth bars, low concrete grade and minimal transverse shear reinforcement. This section describes the use of the existing experimental data from the literature discussed in Section 2 as a basis with which to calibrate numerical models capable of reproducing the observed behavior. As previously highlighted, GLD frame members typically possess smooth reinforcing bars to result in a more pinched hysteretic response. Figure 6(a)

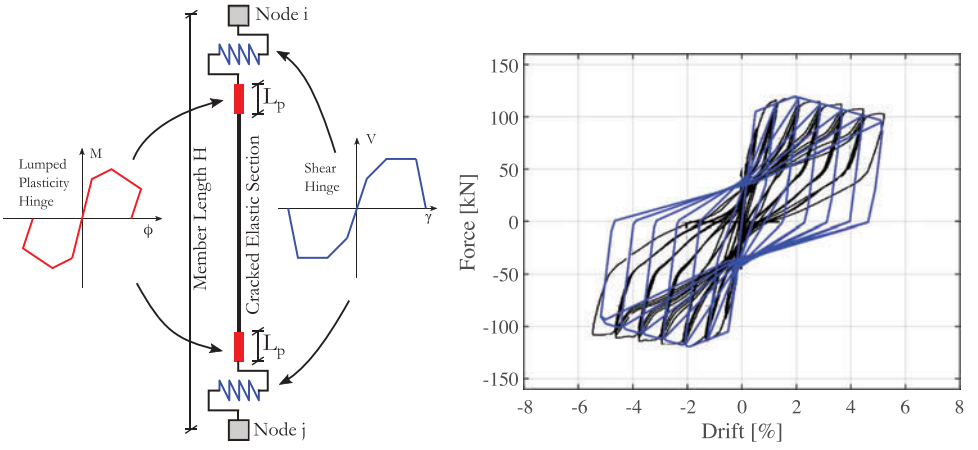

(a) Element model (b) Hysteretic behaviour

Figure 6. (a) Beam-column element model used in this work; a lumped hinge beam-column element to describe the flexural behavior of the member together in series with an aggregated shear hinge that allows for the uncoupled shear response of the member to be accounted for, and (b) illustration of the comparison between the hysteretic behavior of this model and the test specimen R500p-c listed in Table 1.

outlines the proposed numerical modeling approach for these members in OpenSees [McKenna, Fenves, Filippou, and Mazzoni, 2000], where a lumped plasticity element is used to represent the flexural behavior and an uncoupled shear hinge is introduced to capture the shear behavior of the member. In addition, Fig. 6(b) illustrates the comparison between the hysteretic behavior of the proposed model and a sample test specimen from Table 1, where a full comparison with all test specimens is provided in O'Reilly [2016]. The member essentially functions as a classical lumped plasticity member but with an additional hinge definition that allows for a potential shear failure to form at either end of the member due to the additional shear force induced by masonry infill. Since the shear demands induced by the masonry infill will differ at either end of the member during reverse cycle loading, two shear hinges are included at either end to account for the potential shear failure. This is particularly important in the case of Italian construction as the interaction of RC frames with masonry infills has resulted in many cases of short column shear failures in past earthquakes, as discussed in Section 2.1. Again, although it is not discussed in this article, it is anticipated that the effects of masonry infill may be incorporated into the modeling of GLD RC frames using the equivalent diagonal strut modeling approach outlined by Crisafulli, Carr, and Park [2000] with the more recent modifications of Sassun, Sullivan, Morandi, and Cardone [2015], for example, where the interested reader is referred to O'Reilly [2016] for further details of such an implementation.

The available experimental test data discussed in Section 2.2.1 from 23 experimental test specimens [Di Ludovico, Verderame, Prota, Manfredi, and Cosenza, 2013; Melo, Varum, and Rossetto, 2015; Verderame, Fabbrocino, and Manfredi, 2008a; 2008b] has been collected and the parameters pertaining to the backbone behavior of the flexural hinge formed at the base of each specimen have been determined from the information

provided by each test. The results of each test are used to validate the approach described herein and to determine the hysteretic backbone behavior associated with these GLD frame members. A lumped plasticity approach to representing the behavior up to collapse is preferred as a typical fiber-based element approach has been deemed by Haselton, Liel, Taylor Lange, and Deierlein [2008], among others, as being unsuitable to capture the effects of bar buckling and fracture unless special care is taken to incorporate them; an aspect that will be further deliberated in Section 5. This section intends to provide an adequate description of the various parameters such that a user can construct a numerical model, similar to what has been carried out by Haselton, Liel, Taylor Lange, and Deierlein [2008], but for members with non-ductile detailing using a simple and computationally efficient analysis approach. Haselton, Liel, Taylor Lange, and Deierlein [2008] examined a large test database of up to 500 test specimens that allowed for investigation into the effects of many different parameters and subsequent proposal of various predictive equations with multiple variables to account for their influence. However, the available test data for specimens with smooth bars and poor confinement typical of older Italian structures is very limited with respect to this. Therefore, such elaborate predictive equations cannot be reasonably developed until more experimental test data becomes available. The approach of this section is to review the existing approaches and provide a series of simple expressions that can be adopted to predict the backbone behavior reasonably well. By providing simple predictive expressions, assessment of the existing structures can also be performed even when relatively little information regarding cross-sectional detailing is available. This is typically the case when performing an assessment on buildings constructed over 40 years ago where detailed technical information regarding the building's structural design details and reinforcement content is often limited and sometimes not available at all.

As highlighted in Fig. 6, the flexural model consists of a lumped plasticity element with an internal elastic section that is assigned cracked section stiffness properties. Such an element, therefore, requires the definition of a moment-curvature relationship and a plastic hinge length to represent the lumped hinges. Figure 7 shows the basic definition of the hysteretic rule adopted here, which is obtained by using the Pinching4 material model provided in OpenSees.

The yield curvature of the column section can be determined either from moment-curvature analysis or from the simplified expression given in Priestley, Calvi, and Kowalsky [2007] for rectangular RC members as:

$$\phi_y = \frac{2.1\epsilon_y}{h} \qquad \text{(Equation3.1)}$$

where ε_y is the yield strain of the reinforcement and h is the section height. To find M_y, sectional analysis is performed at curvature ϕ_y to find the corresponding bending moment. Comparing the computed yield curvatures and corresponding bending moments to those observed during testing of the 23 test specimens listed in Table 1, the comparison is shown in Fig. 8. Although a high degree of scatter can be observed in the data in both cases, a good match is observed to the point where the above approach is deemed suitable for use in RC members with smooth bars.

Regarding the capping moment (M_c), this term was identified by Haselton, Liel, Taylor Lange, and Deierlein [2008] to be somewhat correlated to the axial load ratio of the

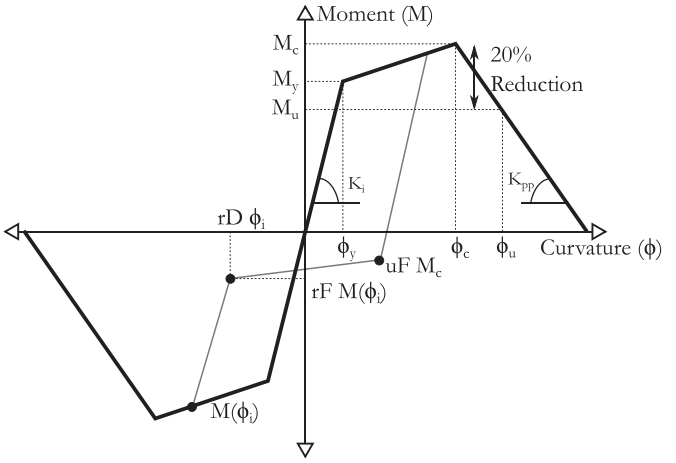

Figure 7. Proposed moment-curvature relationship for beam-column plastic hinge zone, where the behavior is idealized with an initial cracked elastic stiffness to the yield point, followed by plastic deformation to the capping point with a subsequent in-cycle stiffness degradation to represent the loss in strength and stiffness of the member.

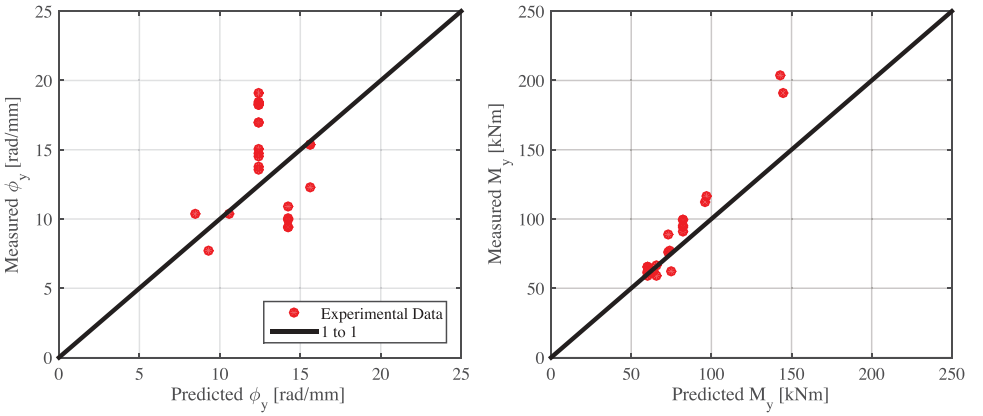

Figure 8. Comparison of the measured yield curvature (left) and bending moment (right) from a total of 23 experimental test specimens to that predicted using Equation 3.1 and sectional analysis, respectively.

member, but examining the ratio of capping to yield moment of the available data, no significant trend was found here. In addition, Haselton, Liel, Taylor Lange, and Deierlein [2008] provided a more simplified form of the equation, where the ratio is simply set to 1.13. Considering that no significant trend with axial load is observed here, it is simply proposed to take the median of the values to give a ratio of $M_c/M_y = 1.077$.

To facilitate the reasonably simple lumped plasticity modeling approach advocated in Fig. 6 and Fig. 7, values for curvature capacity need to be interpreted from the experimental test results, which are typically reported in terms of chord rotations or story drift. In a lumped plasticity approach, plastic deformations are assumed to be concentrated at a

point and the rotation of a plastic hinge is given as the product of the plastic curvature and the plastic hinge length. To this extent, in order to interpret curvature capacities from experimental results, a plastic hinge length expression is needed. Consequently, in this work the plastic hinge length expression of Paulay and Priestley [1992] was selected and used to derive curvature capacities from the experimental results. The plastic hinge length expression of Paulay and Priestley [1992] was developed for members with deformed bars and ductile detailing. As such, its applicability to members with smooth bars is debatable. Considering some of the general observations from the test specimens used here, it was noted that in most cases members with smooth bars tend to form a few large flexural cracks in the plastic hinge zone, as illustrated in Fig. 3. This was specifically highlighted by Di Ludovico, Verderame, Prota, Manfredi, and Cosenza [2013] where a direct comparison between members with deformed and smooth bar specimens showed how deformed bar specimens produced many small cracks in the plastic hinge zone, which allowed the plasticity to spread along the member ends. The corresponding smooth bar specimen, however, was reported by Di Ludovico, Verderame, Prota, Manfredi, and Cosenza [2013] to have developed fewer but larger cracks at the member ends, somewhat restricting the spread of plasticity. This observation would suggest that the above expression for plastic hinge length is not appropriate for RC members with smooth bars. However, experimental testing on an RC beam member by Melo et al. [2011] measured plastic hinge lengths for a beam specimen that correlated reasonably well with the expression from Paulay and Priestley [1992], which suggests it may be reasonable here also. As a general lack of reported plastic hinge lengths from other specimens makes it difficult to propose or validate any alternative expression, the plastic hinge length expression of Paulay and Priestley [1992] is adopted and is currently recommended when modeling the column elements using the approach shown in Fig. 6. Nevertheless, to improve the accuracy of this modeling approach, future research could aim to establish an alternative plastic hinge length expression specifically for columns typical of GLD frames.

Since many of the specimens tested in Europe tend to define the ultimate limit state as the point at which the lateral load capacity has dropped by 20% from its peak capping moment, a third point corresponding to this definition has been highlighted in the descending branch of the backbone curve shown in Fig. 7. As the point corresponds to a 20% loss from the capping moment, its value is already known, leaving just the plastic curvature component to that point to be computed. Considered the use of the Eurocode 8 expressions to compute the ultimate chord rotation capacity of RC members with smooth bars and lap-splices, where a modification was proposed to account for bar lapping. Figure 9 plots the observed ultimate chord rotation to the adjusted expression and the results show that this expression is quite conservative, with a median ratio of measured to predicted of 1.58. This has been subsequently noted by Melo, Varum, and Rossetto [2015], who proposed a correction to the Eurocode 8 expression to account for the increased ultimate chord rotation of members with smooth bars described by:

$$\theta_u = 0.016(0.3)^{\nu}\left(\frac{\max(0.01,\omega')}{\max(0.01,\omega)}f_c'\right)^{0.225}\left(\min\left(\frac{L_s}{h},9\right)\right)^{0.35}25^{\left(\frac{\alpha\rho_v f_{yv}}{f_c'}\right)}1.25^{(100\rho_d)}\left(1.72-0.055\nu^{0.5}f_c'L_s^{0.667}\right) \quad \text{(Equation3.2)}$$

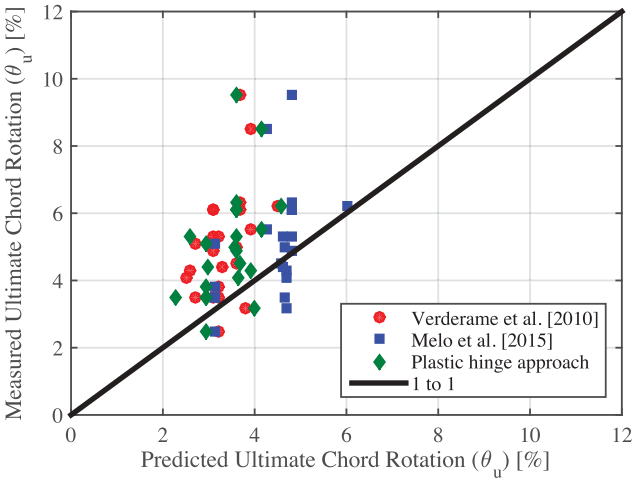

Figure 9. Measured ultimate chord rotation capacity versus predictions from a total of 23 experimental test specimens using empirical approaches by Melo, Varum, and Rossetto [2015] and also a mechanics-based plastic hinge approach. The resulting median ratios of measured-to-predicted are 1.58, 1.11 and 1.41, respectively.

where f_c' is the compressive strength of concrete, L_s is the member shear span, α is the confinement factor, f_{yV} is the strength of the transverse shear reinforcement, ρ_d is the ratio of diagonal reinforcement, and ω' and ω are the normalized ratio of compressive and tensile reinforcement described in Eurocode 8.

While the above approaches rely on a more empirical approach to compute the ultimate chord rotation, a more mechanics-based approach is also investigated here where the ultimate chord rotation is computed using strain-based limit states and the corresponding curvatures and chord rotations are thus found. The strain limit states defined in Paulay and Priestley [1992] are used here, where the minimum curvature corresponding to the concrete and reinforcing steel strains at the extensive damage limit state are used. These correspond to a concrete compressive strain range of ε_c = 0.005–0.01 and reinforcing steel tensile strain of ε_s = 0.015–0.03, respectively. Figure 9 shows the comparison of the ultimate chord rotation predicted using this plastic hinge approach and those observed from testing, where again the prediction appears to be quite conservative with a median ratio of measured to predicted of 1.41. Since the objective of this study is to assess the non-linear behavior of RC members and not to conduct chord rotation validation checks, an adequate representation of the plastic curvature capacity at the ultimate moment is required; hence the proposal by Melo, Varum, and Rossetto [2015] is adopted as it gives the best estimate of ultimate chord rotation from all the approaches considered.

Additionally, Fig. 10 plots the curvature ductility (μ_φ), defined as the ultimate curvature (φ_u) divided by φ_y, against the axial load ratio. From this figure, it is clear that there is a trend of decreasing ductility with increasing axial load ratio in the experimental data (shown in black). The curvature ductility predicted by the other approaches has also been plotted in Fig. 10 along with the median trend line with respect to the axial load ratio. With the objective of providing a simplified relation for the curvature ductility that

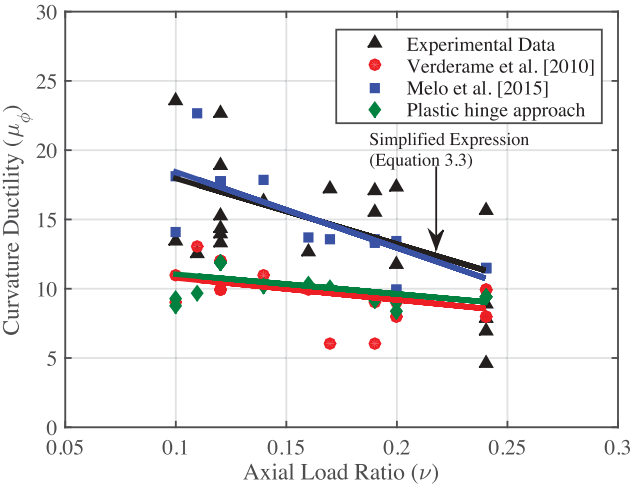

Figure 10. Comparison of the different approaches for computing curvature ductility as a function of axial load ratio, based on a total of 23 experimental test specimens.

depends only on axial load ratio, a least-squares regression fit to the available test data has been undertaken to give:

$$\mu_\phi = 22.7 - 47.4\nu \qquad \text{(Equation3.3)}$$

As expected, there is a degree of scatter in the experimental data but the proposed relation in Equation 3.3 is very close to the expression proposed by Melo, Varum, and Rossetto [2015]. As Equation 3.3 is much simpler, it is proposed as a useful substitute in situations where very few details are known about the beam or column sections to the point where many of the terms required in Equation 3.2 cannot be easily established.

The remaining part of the hysteretic rule shown in Fig. 7 is the definition of the post-capping stiffness K_{pp}. Haselton, Liel, Taylor Lange, and Deierlein [2008] proposed a relation for post-capping rotation capacity as a function of both axial load ratio and transverse shear reinforcement ratio. The dependence on axial load ratio is investigated and plotted in Fig. 11, where the post-capping stiffness computed using the peak and ultimate capacity points of the experimental test specimens outlined in Table 1 is expressed as a ratio to the initial cracked section stiffness K_i ($=M_y/\varphi_y$) through the term a_{pp}. From Fig. 11, an inverse relationship can be seen between the post-capping stiffness ratio and the axial load ratio. As such, the following linear trend line, plotted in Fig. 11, is proposed for determining the post-capping stiffness as a function of the axial load ratio:

$$\mathbf{a_{pp}} = -0.1437\nu - 0.0034 \qquad \text{(Equation3.4)}$$

where a degree of scatter is observed in Fig. 11 that can be quantified by a logarithmic standard deviation of 0.413 assuming a lognormal distribution. The impact of this notable dispersion of the parameter a_{pp} ($=K_{pp}/K_i$), among others, on other aspects of performance such as collapse performance of structures has been studied further in O'Reilly and Sullivan [2017]. As no test data is available for axial load ratios outside the range of 0.1–0.25, the proposed expression should be used within this range and for an axial load ratio outside of this range; the limit value is tentatively suggested.

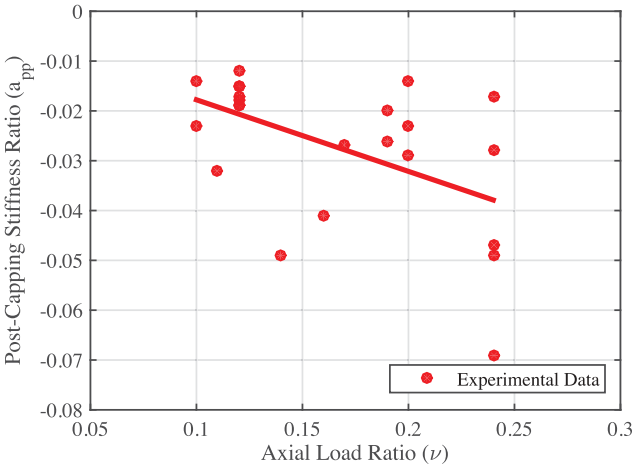

Figure 11. Simplified relation for post-capping stiffness ratio (a_{pp}) defined as a function of axial load ratio based on a total of 23 experimental test specimens.

While the illustration of the moment curvature backbone relationship in Fig. 7 shows the descending branch from M_c to zero moment at a stiffness of K_{pp}, an additional parameter is included in the implementation of this plastic hinge's behavior to account for the potential fracture of the longitudinal reinforcement in members. This stems from the fact that the post-peak stiffness calibration above accounts for the gradual reduction of moment capacity in the members but not the abrupt loss of capacity that would be associated with fracturing of the longitudinal reinforcement. To account for this, a strain-based curvature limit is implemented using the MaxMin material model available in OpenSees, where if the limiting curvature were to be exceeded, the moment capacity would immediately drop to zero. The section curvature corresponding to this limit state is determined from the strain in the longitudinal reinforcement, where a value of $\varepsilon_s = 0.08$ is tentatively proposed based on the values outlined in Priestley, Calvi, and Kowalsky [2007].

It should also be appreciated that while the expressions proposed above are relatively simple and contain some degree of dispersion, this is due to the limited amount of experimental data available to calibrate refined expressions. Ideally, a larger database of experimental testing would be available to perform regression analysis on the data and determine a number of predictor variables for the terms, similar to that performed by Haselton, Liel, Taylor Lange, and Deierlein [2008]. However, since limited information exists and the proposed expressions have been shown to give reasonable predictions when compared to other more elaborate expressions, they may be considered appropriate for structural assessment. Further work by O'Reilly and Sullivan [2017] examines the impact of modeling uncertainty associated with each of these terms on the response and collapse performance. In addition, a benefit of these expressions is that they can also be used even when relatively little information about the actual member section properties is known, as is often the case in assessment of older structures. Cyclic degradation has not been modeled in this work, which has instead relied on the post-peak negative stiffness branch to simulate loss of strength in a structural member. This is supported in the findings of Ibarra, Medina, and Krawinkler [2005] who reported that the actual ductility capacity and

post-peak stiffness are the most influential parameters in assessing collapse, noting that while cyclic degradation is an important parameter, it tends not to be the most critical when assessing collapse. This argument that a cyclic degradation parameter is not a critical issue is further supported by a study by Liel, Haselton, Deierlein, and Baker [2009] on the effects of modeling uncertainty on the collapse fragility of ductile and non-ductile RC frames. For these reasons, it is argued that the omission of a cyclic degradation term is reasonable given that the post-capping stiffness has been defined. Nevertheless, future research could aim to refine the approach used here in order to rigorously capture cyclic degradation effects.

The modeling of the shear deformation in beam-column elements is often omitted as the flexural behavior and deformation are assumed to be the more dominant response mechanism. However, many Italian RC structures have been observed to suffer shear failure either as a result of poor detailing or interaction with the masonry infill. The shear capacity can be computed using advanced mechanics-based approaches such as the modified compression field theory (MCFT) [Vecchio and Collins, 1986], or with more empirical methods, such as the UCSD shear model described in Priestley, Seible, Verma, and Xiao [1993]. While the use of empirical approaches is somewhat undesirable as they remove some of the essence of the mechanics of the failure, methods such as the MCFT provide a rational mechanics-based approach. While it is an attractive approach to computing the shear behavior, the majority of the work conducted on MCFT has been for monotonic loading and it does not directly translate to computing member backbone response for cyclic loading. More recent work by Ruggiero, Bentz, Calvi, and Collins [2016] has examined this difference in monotonic and cyclic shear response experimentally, noting that the shear strength during reverse cycle loading can be as much as 25% lower than the corresponding monotonic one. As a result, Ruggiero, Bentz, Calvi, and Collins [2016] developed a more detailed approach to consider the reverse cycle response of members in shear and validated it with numerous experimental test specimens. However, this approach is rather detailed and difficult to implement in a simple model intended for non-linear response history analysis (NRHA). Hence, a more empirical approach is favored here until a more practice-oriented approach incorporating the findings of Ruggiero, Bentz, Calvi, and Collins [2016] can be developed for members subjected to seismic loading.

Different options are available to numerically model the shear deformations of RC beam-column elements, such as the use of non-linear springs in Elwood and Moehle [2003], for example. The shear modeling approach proposed by Elwood and Moehle [2003] is of limited applicability with respect to GLD RC frames as the user is confined to a single hysteretic model within OpenSees, in addition to the beam-column element being required to have a positive slope in order to obtain a unique solution, leading to potential difficulties when accounting for strength degradation in the plastic hinge regions simultaneously. Given this, the shear force-deformation in GLD RC frames is modeled using an uncoupled shear spring aggregated into the lumped plasticity beam-column element to capture the effects of the shear degradation and failure, similar to previous work on the modeling of short link eccentrically braced steel frames by O'Reilly and Sullivan [2015b]. Through this approach, the failure in shear as a result of masonry infill interaction can be detected during the analysis using a simple and reasonably robust modeling approach and also does away with the need to post-process shear demands in

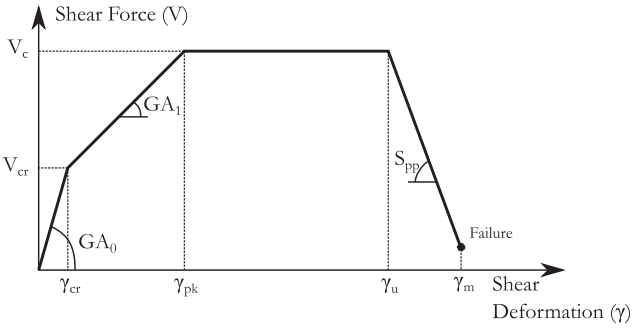

Figure 12. Shear force-deformation backbone hysteresis (Adapted from Zimos, Mergos, and Kappos [2015]).

terms of member capacity. The nature of this uncoupled flexure and shear spring definition implies that members will form the weaker of the two mechanisms and not account for flexure-shear interaction. This assumption is not unreasonable in the case of GLD RC frames with masonry infill as the peak shear force induced by the infill to potentially cause a column shear failure is anticipated to be at relatively low story drifts (<0.5% considering the story drifts corresponding to peak infill force reported by Sassun, Sullivan, Morandi, and Cardone [2015]) compared to the initiation of flexural yielding in column members (typically >1% following the expression provided by Glaister and Pinho [2003]). Therefore, with the aim of accounting for potential column shear failure due to forces induced by masonry infill, the proposed modeling approach is deemed adequate due to the relative gap between the stages of lateral deformation when the two mechanisms may occur for frames with masonry infill. The backbone response of the adopted shear force-deformation is shown in Fig. 12 and consists of 4 phases; the initial elastic behavior, post-cracking, peak response and strength degradation, where the various parameters are determined using the expressions outlined in Mergos and Kappos [2008; 2012] and Zimos, Mergos, and Kappos [2015]. These are based on the UCSD model to compute the capacity (V_c) in addition to empirical fitting for the other relevant terms. Similar to the flexural material model, the onset of failure at a shear deformation of γ_m is implemented through the use of the MaxMin material model in OpenSees where the exceedance of this point results in the abrupt loss of shear capacity in the member.

3.2. *Exterior Beam-Column Joints*

3.2.1. *Shear capacity in Exterior Beam-Column Joints*

The strength of a beam-column joint is characterized by the joint's ability to transfer the shear, flexure and axial forces across the joint. Many shear capacity models have been proposed in the past and vary from empirical approaches to others based on strut-and-tie models or principle stresses. Sharma, Eligehausen, and Reddy [2011] provided a critical review of the existing shear strength models for exterior beam-column joints. In this review, Sharma, Eligehausen, and Reddy [2011] discussed how some empirical approaches have been proposed by authors [Bakir and Boduroğlu, 2002; Hegger, Sherif, and Roesner, 2003], where the models were typically related to parameters such as reinforcement and

joint aspect ratios. More advanced approaches that incorporate the use of a strut-and-tie modeling approach have been proposed by Hwang and Lee [1999]. More recently, Metelli, Messali, Beschi, and Riva [2015] expanded the work of Hwang and Lee [1999] to develop the Modified Softened Strut-and-Tie Model (MSSTM) for exterior beam-column joints with smooth bars and hook-ended anchorage. When comparing the difference between the predicted to observed joint shear capacity in six different experimental test specimens, the approach by Hwang and Lee [1999] showed an average difference of 71.6%, whereas the MSSTM approach by Metelli, Messali, Beschi, and Riva [2015] showed an average difference of 4.4%. This MSSTM method gives very good results in terms of predicting the shear capacity of the joints, although it should be noted that it requires numerous steps of iteration.

A simple mechanics-based approach has been provided in Priestley [1997] for the case of joints with deformed bars and no transverse shear reinforcement, where the use of principle stresses was employed. This is illustrated in Fig. 5, where the principle stresses in the joint at an angle θ are shown. These principle tensile (p_t) and compressive (p_c) stresses are computed directly from consideration of the forces acting on the joint and consider the biaxial stress state caused by the presence of the horizontal and vertical stresses due to column axial load. This model has the advantage of being defined by a number of parameters and was then developed further for the case of smooth hook-ended bars by Pampanin, Magenes, and Carr [2003]. Comparison by Metelli, Messali, Beschi, and Riva [2015] also showed this approach was within 3.2% in terms of predicting joint shear capacity. Sharma, Eligehausen, and Reddy [2011] expanded this general model by Priestley [1997] for principle tensile stresses to consider the effects of the additional net shear force of exterior joints resulting from the beam shear transfer. This approach by Sharma, Eligehausen, and Reddy [2011] results in the need to iterate in order to satisfy equilibrium and introduces a level of complication in what has been otherwise shown to be quite a simple and effective model by Metelli, Messali, Beschi, and Riva [2015]. The following section describes the approach adopted and proposed here using principle tensile stresses. In addition, the beam shear force transfer acting on the joint as outlined by Sharma,

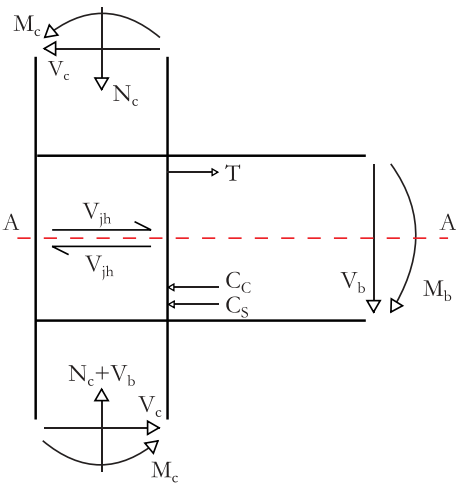

Figure 13. Forces acting within an exterior beam-column joint subassembly.

Eligehausen, and Reddy [2011] is considered, although by assuming that the inflection points of the columns are at mid-height of equal story heights, a closed-form solution requiring no iteration can be obtained.

The layout and forces acting within an exterior beam-column joint are shown in Fig. 13. The equilibrium across Section A-A is found to give the horizontal shear force acting across the joint as V_{jh} = T-V_c. Letting the tensile force in the beam reinforcement (T) be the beam moment M_b over the internal lever arm jd to get T = M_b/jd, taking the joint centre moment M_j as equal to M_b and assuming that the column inflection point is at mid-height of the story height H to give V_c = M_j/H, the following can be written:

$$\mathbf{V_{jh}} \approx \mathbf{M_j}\left(\frac{1}{\mathbf{jd}} - \frac{1}{\mathbf{H}}\right) \qquad \text{(Equation3.5)}$$

By then, taking the horizontal joint shear force as the product of the shear stress (τ_{jh}) and the joint width (b_j) times the depth (h_c), the moment in the joint is given by:

$$\mathbf{M_j} \approx \tau_{\mathbf{jh}}\mathbf{b_j h_c}\left(\frac{\mathbf{Hjd}}{\mathbf{H} - \mathbf{jd}}\right) \qquad \text{(Equation3.6)}$$

where the term τ_{jh} is found by considering the principle tensile stress in the joint.

Evaluation of the vertical forces in Fig. 13 begins with the determination of vertical stress in the joint as the summation of the column axial force (N_c) and the transferred beam shear force (V_b). As previously highlighted by Sharma, Eligehausen, and Reddy [2011] in the context of exterior beam-column frame joints, no equal and opposite beam shear is transferred in exterior joints in Fig. 13 and therefore the total vertical stress in the joint is given by:

$$\sigma_{\mathbf{jv}} = \frac{\mathbf{N_c} + \mathbf{V_b}}{\mathbf{b_j h_c}} \qquad \text{(Equation3.7)}$$

where the V_b term is positive here for the scenario illustrated in Fig. 13. As per Sharma, Eligehausen, and Reddy [2011], the beam shear (V_b) can be related through joint equilibrium to the horizontal shear force by the term α, given by V_b = (h_b/h_c)V_{jh} = αV_{jh}. From this, the resulting vertical normal stress in the joint is substituted to Equation 3.7 to give σ_{jv} = σ_a+ατ_{jh} where σ_a = N_c/$b_j h_c$.

The principle tensile joint stress (p_t) is then found via Mohr's circles of stresses given by:

$$\mathbf{p_t} = \sigma_{\frac{j}{jv/2}} + \sqrt{\left(\frac{\sigma_{\mathbf{jv}}}{2}\right)^2 + \tau_{\mathbf{jh}}^2} \qquad \text{(Equation3.8)}$$

which when substituted with the previous definitions of σ_{jv} and τ_{jh} and rearranging in terms of τ_{jh} gives:

$$\tau_{\mathbf{jh}} = \mathbf{p_t}\frac{\alpha}{2} + \mathbf{p_t}\sqrt{\left(\frac{\alpha}{2}\right)^2 + 1 + \frac{\sigma_{\mathbf{a}}}{\mathbf{p_t}}} \qquad \text{(Equation3.9)}$$

which represents the closed-form solution of the iterative approach outlined in Sharma, Eligehausen, and Reddy [2011] who maintain the tensile force T as a variable to be iterated

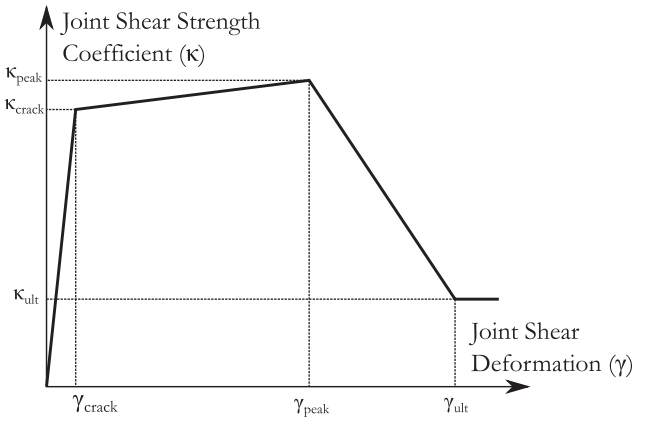

Figure 14. Monotonic backbone curve of beam-column principle tensile stress limit states for exterior beam-column joints.

to find V_c, whereas here the approximation of Equation 3.5 does away with the need to iterate. Substituting in the terms previously defined for the joint moment gives:

$$\mathbf{M_j = p_t b_j h_c \left(\frac{Hjd}{H-jd}\right)\left(\frac{h_b}{2h_c}+\sqrt{\left(\frac{h_b}{2h_c}\right)^2+1+\frac{N_c}{p_t b_j h_c}}\right)} \qquad \text{(Equation3.10)}$$

where the value of p_t for each limit state is determined from comparison with experimental tests by means of a κ coefficient illustrated in Fig. 14 which is related to the tensile strength of the concrete as proposed by Priestley [1997], who proposed a set of coefficients for structures with deformed bars and no joint transverse shear reinforcement. This is represented as $p_t = \kappa(f_c')^{0.5}$. Further experimental work in Pavia, Italy [Calvi, Magenes, and Pampanin, 2002b; Pampanin, Magenes, and Carr, 2003] resulted in a revised set of coefficients for specimens with smooth hook-ended bars compared to those initially outlined by Priestley [1997]. This approach of modeling the points corresponding to cracking and peak force are adopted here, in addition to the introduction of an ultimate strength point to represent the strength and stiffness degradation in the joints. The κ coefficients derived here will differ slightly from those of Pampanin, Magenes, and Carr [2003] as the additional shear force transfer provided by the beam section in Equation 3.7 is considered. The following section will also discuss the determination of the shear deformation at the various limit states previously mentioned. The shear strength of the joint is represented in terms of moment capacity since the numerical modeling employs the use of a zero-length rotational spring since the spring rotation is taken to be equal to shear deformation of the joint, as per previous numerical modeling approaches outlined in Section 3.2.2. Lastly, in terms of hysteretic behavior, three remaining parameters are required for the Hysteretic material model adopted in OpenSees for the beam-column joints – the parameters pinchX and pinchY, which define the pinching behavior during reverse cycles, and the parameter β that modifies the unloading stiffness of the hysteretic behavior.

3.2.2. *Numerical Modeling of Exterior Beam-Column Joints*

Numerical modeling of exterior beam-column joints has received much attention throughout the years, with different approaches varying from single spring model models to more advanced finite element models being proposed. While a critical review of each of the available models in the literature and how these proposals pertain to the numerical modeling of exterior joints would be a welcome discussion here, numerous literature reviews on the past proposals and the evolution in terms of model complexity can be found in the literature [Celik and Ellingwood, 2008; Shafaei, Zareian, Hosseini, and Marefat, 2014; Sharma, Eligehausen, and Reddy, 2011] and are thus omitted here for brevity. In place of this, a brief discussion on some of these existing models that are of direct relevance to the present work is provided.

Many of the more recent models proposed in the literature highlight two main differences when applied to beam-column joints in GLD RC frames in Italy; many of these models are developed for specimens with deformed bars and with different end-anchorage conditions. These are important features as the use of smooth bars greatly increases the bar slip due to a poorer bond which results in an increased lateral deformation of the structure and the use of end-hook anchored bars has been shown by Pampanin, Calvi, and Moratti [2002] to cause a rather brittle joint failure mechanism. As a result of the experimental campaign carried out by Pampanin, Calvi, and Moratti [2002], a numerical model was proposed in Pampanin, Magenes, and Carr [2003] to model the behavior of the beam-column joint. Further work by Galli [2006] showed how a reasonably good estimate could be obtained when compared to the specimens tested by Pampanin, Calvi, and Moratti [2002] and Calvi et al. [2002b]. While this modeling approach for smooth bars with end-hooks worked well in terms of the capacity of the connection, the material model was unable to capture the strength degradation in the joint, which can be significant. Sharma, Eligehausen, and Reddy [2011] proposed a model that considered the shear strength degradation within the joint and compared predictions to experimental results from numerous test specimens with deformed bars and different anchorage conditions. While the results obtained by Sharma, Eligehausen, and Reddy [2011] were very promising in terms of strength and stiffness, the calibration was a monotonic pushover and did not include any specimens with end-hook anchorage.

Using a combination of beam-column elements and joint springs, a model is illustrated in Fig. 15 with which a comparison to the experimental test sub-assemblies available in the literature can be made, where the layout and connectivity of the various elements and springs are shown. The joint region is represented by a series of rigid-link offsets with a lumped rotational spring to represent the shear deformation of the joint region. As previously discussed in Section 3.2.1, the proposed model adopts the approach of using principle tensile stress limit states for the definition of the joint behavior. These principle tensile stress limit states are determined through experimental observation and are expressed as a function of the concrete tensile strength, as initially proposed by Priestley [1997]. The recommended coefficients are given in conjunction with the model described in Section 3.2.1 and the set of proposed coefficients given in Table 2 is based on comparison with experimental test results listed in Table 3. The actual values for κ and γ proposed here are determined based on the median calibrated values outlined later in Section 3.2.3. While there have been many proposals for coefficients for exterior beam-column joints, such as 0.2 by Pampanin, Magenes, and Carr [2003], it must be stated that

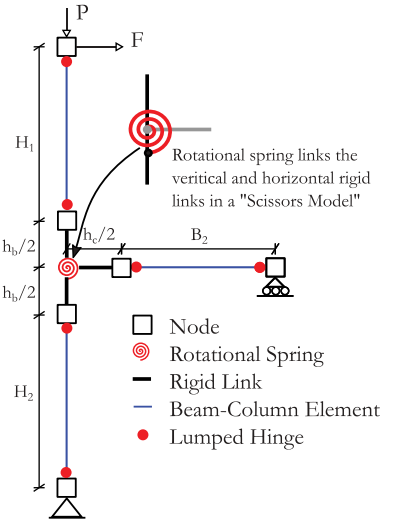

Figure 15. Scissors model layout for exterior beam-column joints.

Table 2. Proposed shear strength coefficient (κ) and shear deformation (γ) values for each limit state in exterior joints.

Limit State	κ	γ [rad]
Cracking	0.135	0.0002
Peak	0.135	0.0127
Ultimate	0.050	0.0200

the values here are slightly lower than these due to the fact that in Section 3.2.1, the proposed model accounts for the contribution of the beam shear force transfer when computing the vertical stress acting in the joint. For the joint shear deformations, the proposed values incorporate the joint rotation caused by diagonal cracking in the joint only and are distinct from the additional plastic hinge deformation at the column and beam member ends. In terms of the joint shear deformation at first cracking, the proposed value of 0.0002 was based on both the observed joint shear deformations reported by past experimental test campaigns (e.g. [Akguzel, 2011; Pampanin, Calvi, and Moratti, 2002]) and also comparison with the overall response of the joint specimen subassemblies, discussed in Section 3.2.3.

Since the shear strength capacity of the rotational spring can be computed using the expressions in Section 3.2.1, the corresponding shear deformation corresponding to each limit state needs to be defined. These limit states are illustrated in the monotonic backbone curve in Fig. 14 and correspond to first cracking of the concrete, peak load and degradation to a residual strength. Some test campaigns have proposed reasonable ranges for the joint shear deformation at various limit states, such as Pampanin, Magenes, and Carr [2003], which are based on visual observation during tests in addition to measured values from testing by Akguzel [2011]. The approach here has been used to calibrate the three limit states shown in Fig. 14 to the existing experimental information and compare these with the existing proposals of shear deformation to finally propose a general set of limit state shear deformations for exterior beam-column joints with smooth end-hook

Table 3. Calibrated shear hinge parameters for exterior beam-column joint specimens.

#	Reference	ID	H [m][1]	B [m][2]	b_b x h_b [cm][3]	b_c x h_c [cm][4]		κ_{crack}	κ_{peak}	κ_{ult}	γ_{peak}[rad]	γ_{ult}[rad]
1	Pampanin, Calvi, and Moratti [2002]	T1	2.49	1.70	20x33	20x20	(-)	0.13	0.13	0.06	0.014	0.020
							(+)	0.11	0.11	0.06	0.015	0.020
2	Pampanin, Calvi, and Moratti [2002]	T2	2.49	1.70	20x33	20x20	(-)	0.13	0.13	0.05	0.009	0.020
							(+)	0.11	0.11	0.05	0.009	0.020
3	Braga, Gigliotti, and Laterza [2009]	T23-1	2.20	1.42	20x33	20x20	(-)	0.11	0.11	0.05	0.018	0.020
							(+)	0.12	0.12	0.05	0.015	0.023
4	Melo, Varum, Rossetto, and Costa [2012]	TPA-2	3.00	2.00	24x40	25x25	(-)	0.14	0.14	0.05	0.012	–
							(+)	0.14	0.14	0.05	0.012	–
5	Melo, Varum, Rossetto, and Costa [2012]	TPB-2	3.00	2.00	25x40	25x25	(-)	0.14	0.14	0.06	0.016	–
							(+)	0.14	0.14	0.06	0.016	–
6	Melo, Varum, Rossetto, and Costa [2012]	TPC	3.00	2.00	25x40	25x25	(-)	0.11	0.11	0.05	0.007	0.016
							(+)	0.11	0.11	0.05	0.007	0.016
7	Akguzel [2011]	2D1	2.00	1.52	23x33	23x23	(-)	0.20	0.20	0.05	0.015	0.020
							(+)	0.18	0.18	0.06	0.015	0.020
8	Akguzel [2011]	3D1x	2.00	1.52	23x33	23x23	(-)	0.16	0.16	0.05	0.012	–
							(+)	0.14	0.14	0.05	0.012	–
9	Akguzel [2011]	3D1y	2.00	1.52	23x33	23x23	(-)	0.14	0.14	0.05	0.012	–
							(+)	0.14	0.14	0.05	0.012	–
10	Beschi, Riva, Metelli, and Meda [2014]	CJ	3.00	2.25	30x50	30x30	(-)	0.12	0.12	0.05	0.018	–
							(+)	0.12	0.12	0.05	0.018	–

[1] Referring to Fig. 15, $H = H_1+H_2+h_b$
[2] Referring to Fig. 15, $B = B_2 + 0.5h_c$
[3] b_b and h_b refer to the beam width and height, respectively.
4 b_c and h_c refer to the column width and height, respectively.

anchorage. These proposed values are summarized in Table 2. The joint shear deformation at cracking has been set at 0.0002 radians as initially proposed by Pampanin, Magenes, and Carr [2003] since, as will be seen in the following section, this value gives quite good results in terms of matching the initial stiffness of the model and experimental test data. However, one parameter which may lead to an increase in the value for joint shear deformation at cracking is the axial load ratio. This trend was highlighted in a numerical parametric study by Genesio [2012] and also in the approach proposed by Metelli, Messali, Beschi, and Riva [2015]. However, since the axial load ratio of the specimens tested here was quite low and relatively constant (ν between 0.06–0.21 with a mean of 0.12), it was rather difficult to confirm this trend from experimental data, so much so as to warrant inclusion in the limit state definition. This trend also applies to the other limit states and is stated here to be an area that needs further work to clarify a more refined trend. Similarly, Genesio [2012] and Metelli, Messali, Beschi, and Riva [2015] both noted a dependence of the joint shear deformation limit states on beam to column height ratios, but due to the relatively constant ratios in the test data here, it was again deemed inappropriate to define this dependency.

Comparing the proposed shear deformations at peak load (see Fig. 14) to that of the measurements of the "2D1" specimen reported in Akguzel [2011], the value proposed for the joint shear deformation here match well with this specimen's response in that the principle tensile stress capacity begins to degrade at roughly the same shear deformation proposed here. Similarly, the values proposed in Pampanin, Magenes, and Carr [2003], which are based on test observations suggests that extensive damage and reparability issues arise at deformation levels between 0.01 and 0.015 radians, where deformations exceeding 0.015 radians were noted to lead to incipient collapse. Comparing these values with those of Table 2 shows that the proposed values for the defined limit states match reasonably well, with the proposed value for peak and ultimate response falling within the ranges initially proposed by Pampanin, Magenes, and Carr [2003]. Therefore, these values of joint shear deformation in Table 2 are seen to be consistent with experimentally measured values.

Similar to the case of the beam-column elements, an upper bound on the joint shear deformation may be tentatively suggested to account for the possible collapse of the beam-column joint. As no experimental test specimen was reported to have collapsed, a preliminary value of joint shear deformation may be approximated using the MSSTM outlined in Section 2.1.2 of Metelli, Messali, Beschi, and Riva [2015] and summarized by the following expression:

$$\gamma_{\mathbf{max}} = 0.5\left(\zeta\epsilon_{\mathbf{cu}} + \frac{\mathbf{w_u}\sin(\theta_j)}{\mathbf{h_j}}\right)\left(\tan(\theta_j) + \frac{1}{\tan(\theta_j)}\right) \qquad \text{(Equation3.11)}$$

where ζ is the concrete softening coefficient, ε_{cu} is the ultimate concrete compressive strain, w_u the diagonal crack width, h_j and θ_j are the height and inclination of the joint diagonal strut, respectively. Taking the concrete compressive strain ε_{cu} as 0.02, the softening coefficient as 0.55 and the diagonal crack width at collapse as 2 mm, as suggested by Metelli, Messali, Beschi, and Riva [2015], the corresponding joint shear deformation can be computed for the T1 specimen in Table 3 to be approximately 0.024, for example. This approach may be tentatively adopted to compute a joint shear deformation with which to

apply the MaxMin limits in OpenSees after which the joint strength is reduced to zero to account for the collapse of the beam-column joints. However, it must be emphasized that this represents an approximate approach and experimental testing to better quantify this joint collapse is required in future research.

3.2.3. *Comparison with Experimental Test Results*

Using the model previously described, this section collects and presents the available test data on exterior beam-column joints with smooth end-hooked bars and no transverse shear reinforcement in the joint. The results from each of these tests are then compared with that of the model described earlier, where a number of parameters outlined in Fig. 14 are calibrated. Table 3 outlines a total of 10 experimental tests on exterior joint specimens constructed with smooth bars with end-hooks available in the literature and representative of older GLD RC frames discussed here. For each of the specimens listed in Table 3, a numerical model was constructed according to the layout shown in Fig. 15 and a quasi-static cyclic pushover analysis was performed. The parameters associated with the strength and deformation capacity of the rotational shear hinge were then calibrated based on comparison with the observed test data. The hysteretic backbone parameters used for each of the test specimens are given in Table 3 and using these parameters the comparative plots are made in Fig. 16 and Fig. 17, where the reference of each test is given above each subplot.

Comparing the numerical models with the experimental data in Fig. 16 and Fig. 17, it can be seen that the overall matching is quite good. The backbone matches well in terms of initial stiffness and strength envelope including the degradation of the test specimens at large shear deformation. In addition, the hysteretic behavior is quite good, as the pinching behavior of the specimens is modeled well and the stiffness transitions between positive and negative loading matching. Also, the unloading stiffness of the specimens is well represented by the fact that the β factor used in the Hysteretic material model was set to allow a gradual degradation of the unloading stiffness with increasing ductility. The coefficients adopted in each case for the hysteretic parameters pinchX, pinchY, and β were 0.6, 0.2, and 0.3, respectively. Finally, in terms of the initial stiffness of the joint specimens, the proposed value for γ_{crack} of 0.0002 radians is reasonable when comparing the overall response of the test specimens and also the measured joint shear deformation values reported by test campaigns such as Akguzel [2011] for specimen 2D1, for example.

4. Comparison with Test Frame Specimens

The previous sections provided a number of recommendations for the modeling and analysis of GLD RC frames. In order to further validate the approach, a comparison between the responses of two three story frame structures is presented herein. The global response and the observed local damage pattern of the frames, which were tested both pseudo-statically and pseudo-dynamically will be examined.

4.1. *SPEAR Test Frame*

The first of these specimens is the SPEAR test frame examined by Negro, Mola, Molina, and Magonette [2004], possessing the general layout shown in Fig. 18. Although the

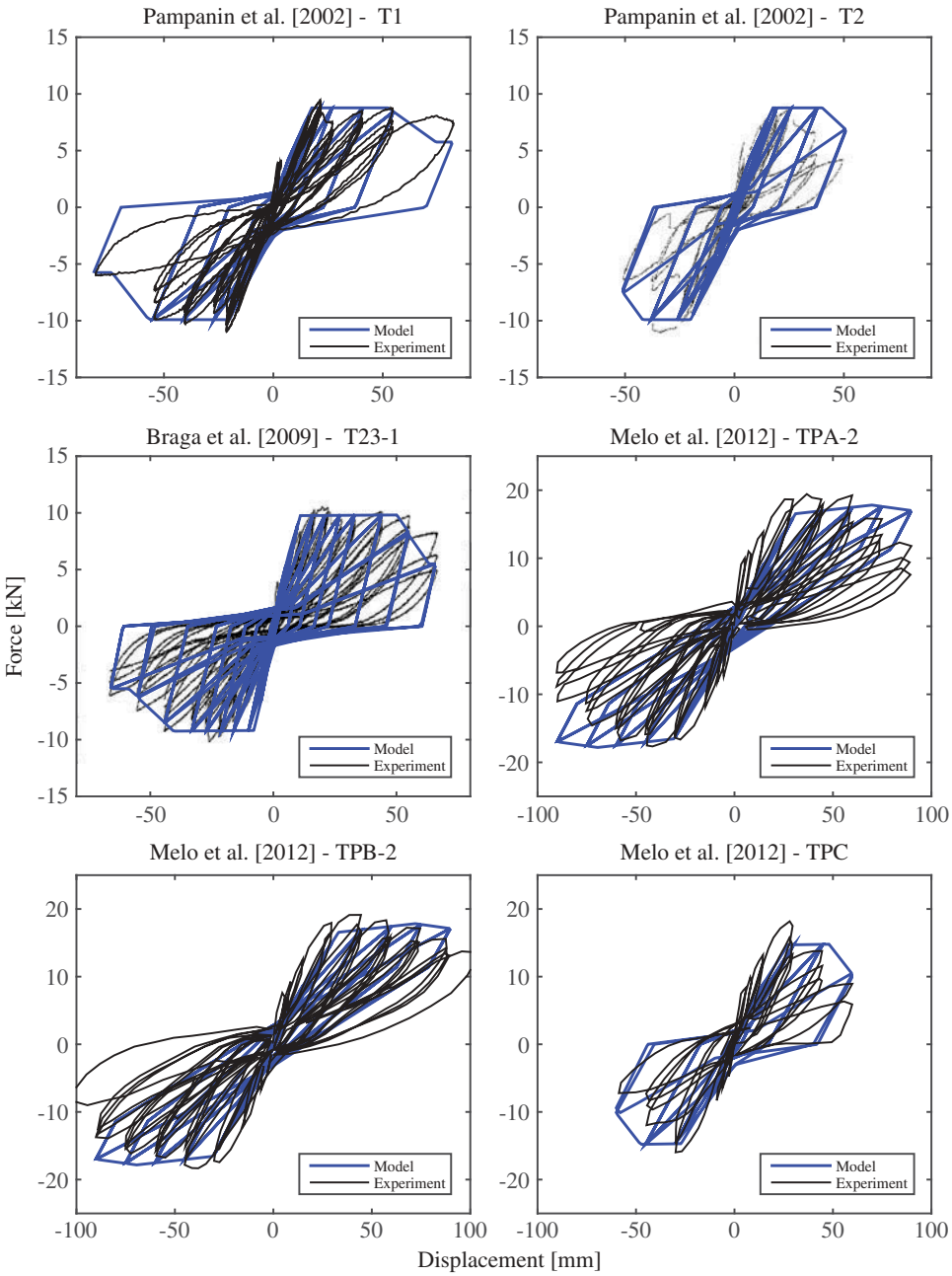

Figure 16. Cyclic pushover comparison of experimental and numerical model on exterior joints.

structure has been designed to the Greek design code in place between 1954 and 1995, it bears many similarities to the same construction practice across much of southern Europe including Italy as the structure was designed to resist vertical gravity loading only, had poor structural configuration considerations in addition to a lack of capacity design principles that form the basis of modern seismic design codes. Negro, Mola, Molina,

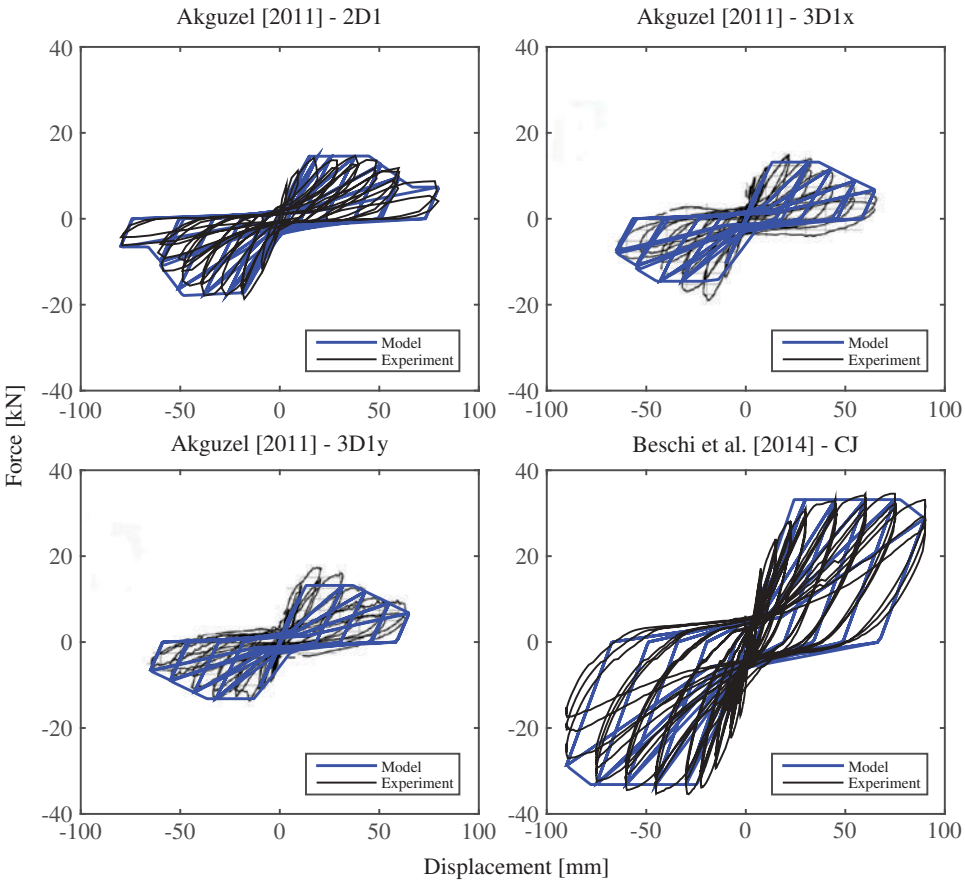

Figure 17. Cyclic pushover comparison of experimental and numerical model on exterior joints.

and Magonette [2004] described the full scale specimen without masonry infills tested using pseudo-dynamic testing at the ELSA Laboratory in Ispra, Italy in 2004. The structure was doubly asymmetric meaning that torsional response was expected to be significant. The test specimen was bi-directionally excited with four actuators and further details of the test setup are provided in Molina, Verzeletti, Magonette, Buchet, and Géradin [1999]. The ground motion record used was from the 1979 Montenegro event and was spectrally adjusted to be compatible with the Eurocode 8 soil type C design spectrum.

At the beginning of the experimental campaign, a low intensity of 0.02 g PGA was run in order to identify the elastic dynamic properties of the structure. From this, Negro, Mola, Molina, and Magonette [2004] described how two intensities of 0.15 g and 0.20 g PGA were subsequently conducted, where an insufficient level of damage during the first test indicated that a stronger intensity was required. The damage was mainly confined to the square columns on the ground floor. Some cracking was shown in the beam members around the strong column member C6 (see Fig. 18). No damage was reported in the beam-column joints. Differences in the center of mass (COM) displacements and the

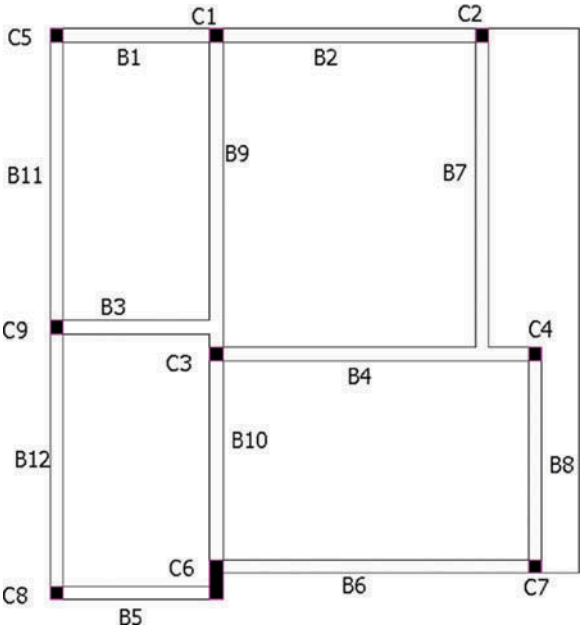

Figure 18. Plan layout of SPEAR frame tested by Negro, Mola, Molina, and Magonette [2004] at the ELSA Laboratory in Ispra, Italy.

different column displacements were highlighted during the test and the torsional response showed some columns actually suffered more damage than the others. This highlights the need to not just consider the COM response in assessment of torsionally sensitive buildings, as deliberated in O'Reilly, Sullivan, and Filiatrault [2017].

A numerical model was built using the approaches described in Section 3 for the test specimen. The irregular nature of the column and beam connectivity was considered via the use of rigid-end offsets in the beam and column members. The base connection as considered fully fixed and the slab system was represented using a rigid diaphragm. P-Delta effects were considered through the application of the tributary gravity loading to each of the column members. The effective width of the T-flanged beam members was computed using the recommendations outlined in Paulay and Priestley [1992], with the yield curvature of the section computed using the expression outlined in Priestley, Calvi, and Kowalsky [2007] for T-flanged beam members. The models were analyzed using the cracked section stiffness properties and a Rayleigh damping model was adopted with 3% of critical damping defined for the first and third modes. This damping value is adopted based on the measured values during the initial characterization tests described by Negro, Mola, Molina, and Magonette [2004].

Figure 19 compares the experimentally observed displacements and the numerical modeling predictions for both the 0.15g and 0.20g PGA intensity levels. The maximum displacements in the X direction are matched excellently, whereas the displacements in the Y direction and the torsional response are slightly underestimated, but still reasonably representative. Considering that the modeling prediction presents the as-is blind prediction of the response using the proposed procedure and does not contain any adjustment

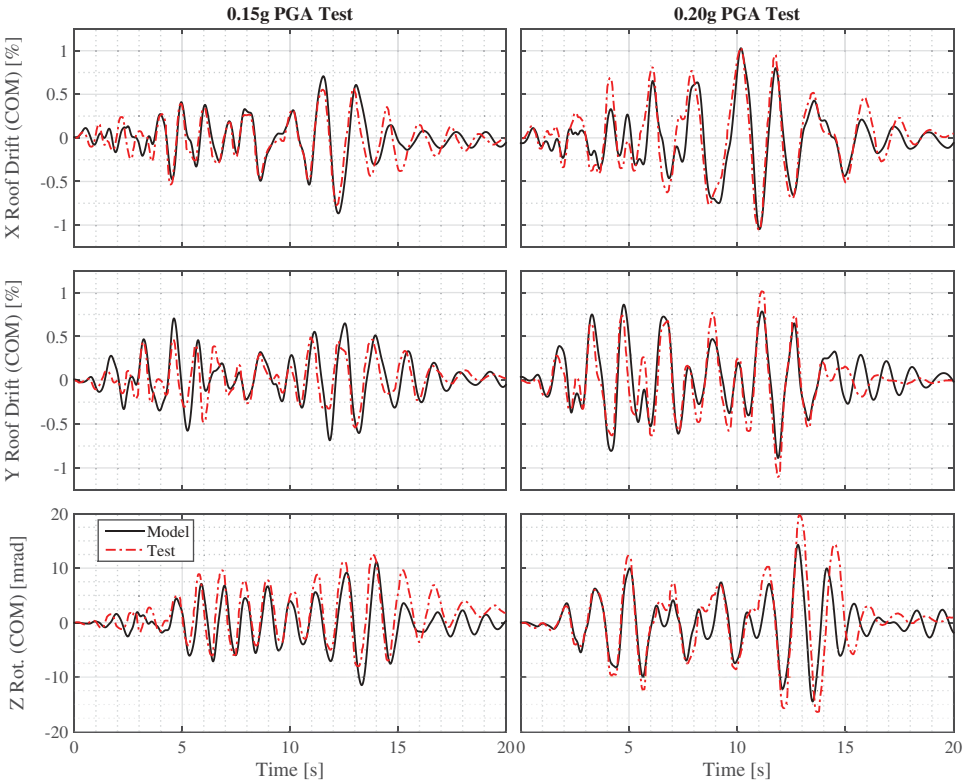

Figure 19. Comparison of the recorded displacements and COM rotation at the roof level from both the 0.15g and 0.20g PGA tests with the results obtained using the adopted numerical modeling strategy for GLD RC frames.

or refinement of the parameters, it can be seen that the predictive capability of the proposed modeling approach is quite good. Negro, Mola, Molina, and Magonette [2004] report that at the end of testing the damage to the structure was mainly confined to flexural cracking at the ends of the column members at the ground floor, with some spalling at the ends of column C3. Some cracking was observed in the slab and beams in the vicinity of the larger column C6 and no damage was observed in the beam-column joint regions. Comparing these test observations with the damage observed in the numerical prediction showed a similar damage pattern with light damage to the column ends, no damage recorded in the beam-column joints and some light damage to beams in the vicinity of column C6.

4.2. *Calvi et al. [2002] Test Frame*

The test campaign carried out by Calvi et al. [2002b] looked at the response of a 2/3 scale three story RC frame detailed for gravity loading only, representing a typical RC frame structure constructed in Italy prior to the introduction of seismic codes around the 1970s. The structure was designed using the Regio Decreto [1939] standard and other relevant design manuals summarized in Vona and Masi [2004] to be representative of construction

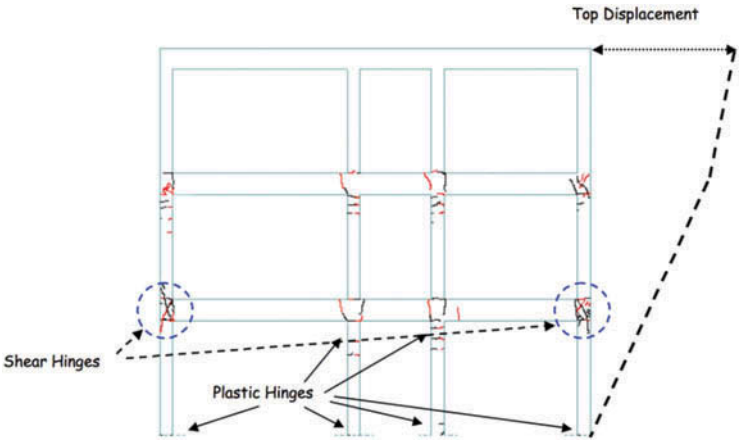

Figure 20. Crack damage reported by Calvi et al. [2002b] at a roof drift of 1.6%.

practice at the time in Italy. The frame was constructed using smooth reinforcing bars terminated with end-hooks in the exterior beam-column joints and longitudinal column bar lapping just above the joint region. Further details regarding the frame test setup can be found in Calvi et al. [2002b] .

The quasi-static cyclic testing of the three-story structure demonstrated the brittle behavior of the exterior joints and interior column members. This is evident from the crack pattern shown in Fig. 20, which shows that the damage was heavily concentrated in the exterior joints on the first floor of the structure. At these joint locations the concrete wedge mechanism reported from sub-assembly test specimens tested by Pampanin, Calvi, and Moratti [2002] was also observed for the whole frame. This resulted in the formation of a shear hinge mechanism, which spreads the joint deformation over the adjacent floors, as opposed to concentrating the damage in a single story, as would have been the case had a soft story mechanism formed due to flexural yielding at the column ends.

Using the frame geometry, reinforcement layout and material properties reported in Calvi et al. [2002b] and the proposed parameters for the beams, column and joints proposed in Section 3, a model of the frame is constructed and subject to a cyclic pushover analysis that consist of a series of three cycles at increasing levels of roof drift (±0.1%, 0.2%, 0.6% and 1.2%) with one final cycle at ±1.6%. This numerical model along with a set of additional scripts to implement the modeling approach outlined in this article is available at: https://github.com/gerardjoreilly/Numerical-Modelling-of-GLD-RC-Frames.

The predicted response is seen in Fig. 21(a) to be very good in general, with the yield force of the structure well represented along with the gradual degradation of the frame resistance at higher displacement levels. The hysteretic response of the structure in Fig. 21 (a) is also well represented, both in terms of the unloading stiffness and pinching and also during the reloading phases of the response. A comparison between the observed displaced shape and the numerical model prediction at a number of different roof displacement levels is shown in Fig. 21(b). The overall matching of the displaced shape is excellent, with the evolution of the displaced shape being tracked well for each cycle. This is particularly evident in the way the shear hinge in the first floor resulting in a spread of

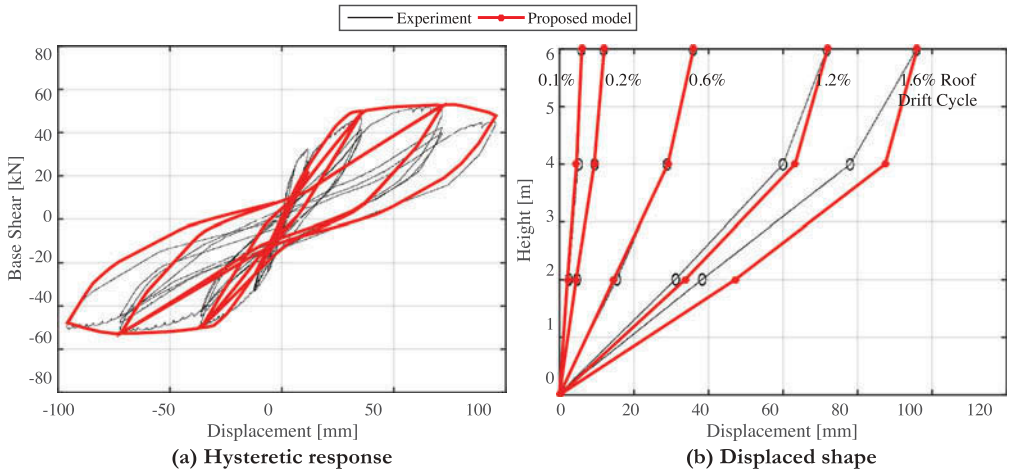

Figure 21. Comparison of predicted pushover response of the three-story frame to the observed test results in (a), where the displacement profiles at each of the peak roof drift cycles are also shown in (b).

deformation over the two adjacent floors. This highlights the proposed model's ability to adequately represent the mechanism typically found in older GLD frames in Italy.

5. Relative Impacts of Modeling Decisions

The previous sections have described the implementation of a numerical modeling approach for GLD RC frames, where the individual components were examined in Section 3 followed by two different three story specimens in Section 4. Good matching was observed for the two frames in Section 4 to illustrate the ability of the proposed modeling approach to capture the different particularities of the GLD RC frame behavior in terms of both hysteretic behavior and displaced shape. This section presents a brief comparison by taking two more conventional methods of analysis that are used for modeling modern RC frames where no attention was paid to the different aspects of GLD RC frame response and the relative impacts on the predicted response are illustrated. Similar work has been carried out by O'Reilly and Sullivan [2015], among others, to examine the impacts of modeling decisions on the response of a simple case study structure to numerous ground motions, although the study here focuses solely on the cyclic pushover analysis of the frame described in Section 4.2, so that comparisons with actual experimental test observations can be made.

The first of these comparisons is using the lumped plasticity model calibrated by Haselton, Liel, Taylor Lange, and Deierlein [2008] whose hysteretic backbone has been calibrated using numerous experimental test specimens on ductile beam-column members with deformed bars. The second comparison consists of using a force-based fiber element approach for the beam and column members, where the cross section is discretized into a number of fibers to represent the constitutive material behavior of both the concrete and reinforcing steel. Both approaches represent reasonable ways in which to model a more modern RC frame with seismic design provisions and adequate member detailing. No particular attention has been paid to the modeling of the beam-

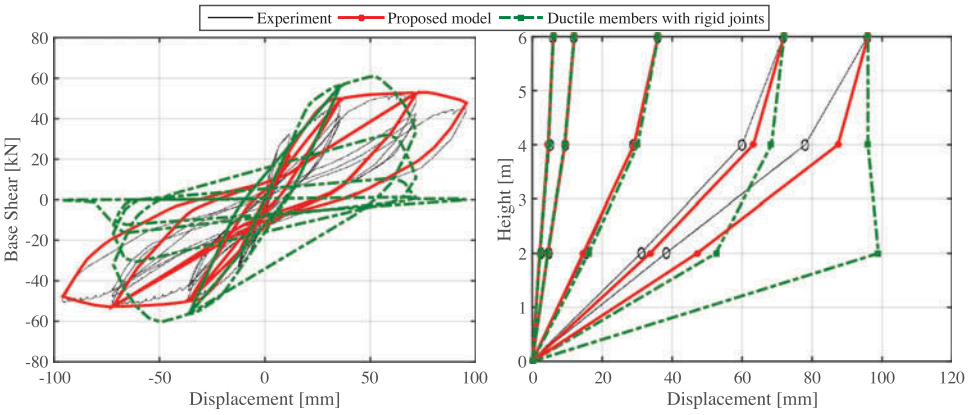

(a) Ductile members with rigid joints.

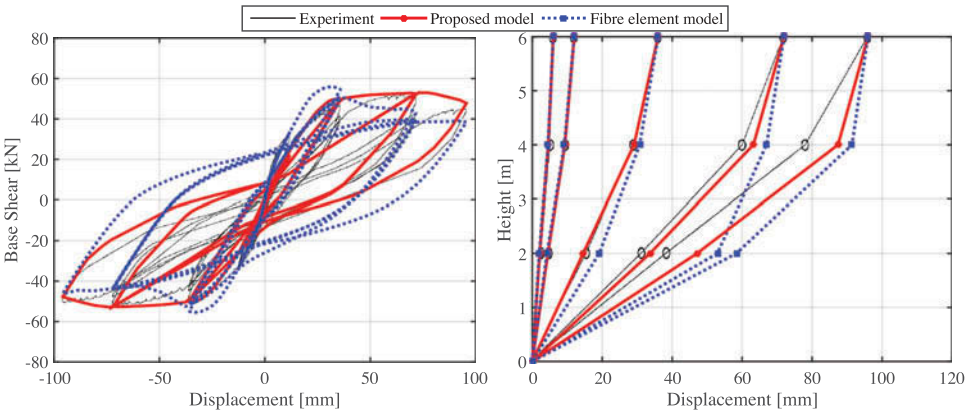

(b) Force-based fibre element with rigid joints.

Figure 22. Comparison of global hysteretic response of the test frame described in Calvi et al. [2002b] and the displacement profile at various stages of the test with the two conventional modeling approaches considered, where the proposed model's prediction is also included to illustrate the improved prediction.

column joint regions and the rigid offsets of the beam and column members have been adopted.

The difference in response of both approaches is immediately obvious from the push-over curves shown in Fig. 22, where the use of the lumped plasticity elements actually results in a reduced global displacement capacity, whereas the fiber elements modeled shows much fatter hysteretic loops without a significant degradation of the strength or stiffness after numerous cycles of loading. Upon closer examination of the displaced shape, the cause of this apparent non-ductile response in Fig. 22(a); is due to the formation of a soft story mechanism in the ground floor of the structure, therefore concentrating the damage entirely on this floor. Comparing this to the proposed model, where the formation of a shear hinge in the joints resulted in the spread in deformation over the two adjacent storys to result in a more stable response of the structure. This highlights that even though the detailing of the members may be insufficient by modern design code standards, the response of the structure may not necessarily be worse as the joint mechanism alters the

global structural response. The fiber element model, on the other hand, shows a reasonable comparison if one were to consider just the envelope of the response. However, the stiffness transitions between cycles are not well represented resulting in a much fatter hysteretic loop and consequently increased hysteretic energy dissipation compared to the actual test specimen. Again, the fiber element model does not capture the occurrence of the joint shear mechanism either and does not exhibit a soft story response as was the case with the lumped plasticity elements. This can be attributed to the lack of any special attention to incorporate the post-peak strength and stiffness degradation in the column members at the ground floor.

6. Conclusions

The structural components that have been shown during past earthquakes in Italy to be vulnerable to non-ductile modes of response in GLD RC frames have been discussed. These include the column members, which have been seen to be vulnerable to damage through a lack of capacity design in GLD RC frames such that a column sway mechanism is often expected, or shear failure due to interaction with masonry infill. A means of modeling these members in OpenSees has been described and calibrated using available experimental test data of column members with older design and detailing. In particular, the modeling approach is able to account for the presence of smooth bars and poor confinement, which are known to affect the behavior of columns in terms of more pinched hysteretic properties and strength degradation. Furthermore, the potential shear failure of the column members has been incorporated through the inclusion of an uncoupled shear spring at the member ends. In addition to the column members, exterior beam-column joints in GLD RC frames have been shown in the past to be quite vulnerable to damage. Their behavior has been included in the proposed modeling approach through the use of a scissors beam-column joint model, whereby the backbone behavior of this model has been determined by considering the principle tensile stresses in the joint and calibrating coefficients using available test data.

Combining these different developments for the modeling of GLD RC frames, comparisons were made between two different three story frame specimens tested both pseudo-statically and pseudo-dynamically. Comparing with the specimen tested by Calvi et al. [2002b], the proposed numerical model tracked the evolution of the deformed shape with every increasing cycle of lateral displacement excellently, noting that the formation of a shear hinge in the first floor and resulting spread in deformation over the two adjacent floors was captured. The initial stiffness, overall lateral strength, and pinching behavior were also very well represented by the model. Comparison with the pseudo-dynamic response of the specimen tested by Negro, Mola, Molina, and Magonette [2004] further illustrated that the numerical modeling approach proposed here can be used to model the response of GLD RC frames subject to dynamic excitation.

Lastly, a comparison of the relative impacts of two different models with ductile RC frame members was carried out to illustrate what the predicted response would have been if an analyst were not to consider the various particularities of GLD RC frame behavior through the adoption of models more suited to modern RC frames with ductile detailing. This was shown to have a significant effect on the response, with the overall mechanism not being captured in addition to the hysteretic behavior not being well represented. This

further highlighted that numerical modeling approaches capable of representing the overall behavior and damage mechanisms are a critical aspect for the seismic assessment of GLD RC frames.

Acknowledgments

The first author would like to acknowledge the funding provided by the IUSS Pavia doctoral programme. The test data provided by Matteo Moratti, Consuelo Beschi, and Paolo Negro is also gratefully acknowledged.

References

Akguzel, U. [2011] "Seismic performance of FRP retrofitted exterior RC beam-column joints under varying axial and bidirectional loading," PhD Thesis, University of Canterbury, New Zealand.

Augenti, N. and Parisi, F. [2010] "Learning from construction failures due to the 2009 L'Aquila, Italy, Earthquake," *Journal of Performance of Constructed Facilities* **24**(6), 536–555.

Bakir, P. G. and Boduroğlu, H. M. [2002] "A new design equation for predicting the joint shear strength of monotonically loaded exterior beam-column joints," *Engineering Structures* **24**(8), 1105–1117.

Beschi, C., Riva, P., Metelli, G. and Meda, A. [2014] "HPFRC jacketing of non seismically detailed RC corner joints," *Journal of Earthquake Engineering* **19**(1), 25–47.

Braga, F., Gigliotti, R. and Laterza, M. [2009] "R/C existing structures with smooth reinforcing bars: experimental behaviour of beam-column joints subject to cyclic lateral loads," *The Open Construction and Building Technology Journal* **3**(1), 52–67.

Bursi, O. S., Dusatti, T. and Pucinotti, R. [2009] *A Reconnaissance report*. 6 April 2009, L'Aquila Earthquake. Italy.

Calvi, G. M., Magenes, G. and Pampanin, S. [2002a] "Relevance of beam-column joint damage and collapse in RC frame assessment," *Journal of Earthquake Engineering* **6**(Supp 1), 75–100.

Calvi, G. M., Magenes, G. and Pampanin, S. [2002b] "Experimental test on a three storey RC frame designed for gravity only," *12th European Conference on Earthquake Engineering*, London, UK.

Celano, F., Cimmino, M., Coppola, O., Magliulo, G. and Salzano, P. [2016] "Report dei danni registrati a seguito del terremoto del Centro Italia del 24 Agosto 2016," *ReLUIS Report (Release 1)*.

Celik, O. C. and Ellingwood, B. R. [2008] "Modeling beam-column joints in fragility assessment of gravity load designed reinforced concrete frames," *Journal of Earthquake Engineering* **12**(3), 357–381.

Crisafulli, F. J., Carr, A. J. and Park, R. [2000] "Analytical modelling of infilled frame structures - A general review," *Bulletin of the New Zealand Society for Earthquake Engineering* **33**(1), 30–47.

Del Gaudio, C., De Martino, G., Di Ludovico, M., Manfredi, G., Prota, A., Ricci, P. and Verderame, G. M. [2016] "Empirical fragility curves from damage data on RC buildings after the 2009 L'Aquila earthquake," *Bulletin of Earthquake Engineering* **15**(4), 1425–1450.

Di Ludovico, M., Verderame, G. M., Prota, A., Manfredi, G. and Cosenza, E. [2014] "Cyclic behavior of nonconforming full-scale RC columns," *Journal of Structural Engineering* **140**(5).

Elwood, K. J. and Moehle, J. P. [2003] "Shake table tests and analytical studies on the gravity load collapse of reinforced concrete frames," *PEER Report 2003/01*, Berkeley, California.

EN 1998-3:2005. [2005] *Eurocode 8: Design of Structures for Earthquake Resistance - Part 3: Assessment and Retrofit of Buildings*, Brussels, Belgium.

EN 1998-3:2009. [2009] *Corrigenda to EN 1998-3*, Brussels, Belgium.

Galli, M. [2006] "Evaluation of the seismic response of existing RC frame buildings with masonry infills," MSc Thesis, IUSS Pavia, Italy.
Genesio, G. [2012] "Seismic assessment of RC exterior beam- column joints and retrofit with haunches using post-installed anchors," PhD Thesis, Universitat Stuttgart, Germany.
Glaister, S. and Pinho, R. [2003] "Development of a simplified deformation-based method for seismic vulnerability assessment," *Journal of Earthquake Engineering* **7**(sup001), 107–140.
Haselton, C. B., Liel, A. B., Taylor Lange, S. and Deierlein, G. G. [2008] "Beam-column element model calibrated for predicting flexural response leading to global collapse of RC frame buildings," *PEER Report 2007/03*, Berkeley, California.
Hegger, J., Sherif, A. and Roesner, W. [2003] "Nonseismic design of beam–column joints," *ACI Structural Journal* **100**(5), 654–664.
Hwang, S. J. and Lee, H. J. [1999] "Analytical model for predicting shear strength of exterior RC beam column joints for seismic resistance," *ACI Structural Journal* **96**(5), 846–857.
Ibarra, L. F., Medina, R. A. and Krawinkler, H. [2005] "Hysteretic models that incorporate strength and stiffness deterioration," *Earthquake Engineering & Structural Dynamics* **34**(12), 1489–1511.
ISTAT. [2011] "Censimento della popolazione e delle abitazioni 2011, Censimento Popolazione Abitazioni, 25 October 2016." Retrieved from http://dati-censimentopopolazione.istat.it/Index.aspx#
Landi, L., Tardini, A. and Diotallevi, P. P. [2016] "A procedure for the displacement-based seismic assessment of infilled RC frames," *Journal of Earthquake Engineering* **20**(7), 1077–1103.
Liel, A. B., Haselton, C. B., Deierlein, G. G. and Baker, J. W. [2009] "Incorporating modeling uncertainties in the assessment of seismic collapse risk of buildings," *Structural Safety* **31**(2), 197–211.
McKenna, F., Fenves, G., Filippou, F. C. and Mazzoni, S. [2000] "Open system for earthquake engineering simulation (OpenSees)," http://opensees.berkeley.edu/wiki/index.php/Main_Page.
Melo, J., Fernandes, C., Varum, H., Rodrigues, H., Costa, A. and Arêde, A. [2011] "Numerical modelling of the cyclic behaviour of RC elements built with plain reinforcing bars," *Engineering Structures* **33**(2), 273–286.
Melo, J., Varum, H. and Rossetto, T. [2015] "Experimental cyclic behaviour of RC columns with plain bars and proposal for Eurocode 8 formula improvement," *Engineering Structures* **88**, 22–36.
Melo, J., Varum, H., Rossetto, T. and Costa, A. [2012] "Cyclic response of RC beam-column joints reinforced with plain bars : an experimental testing campaign," *15th World Conference on Earthquake Engineering*, Lisbon, Portugal.
Mergos, P. E. and Kappos, A. J. [2008] "A distributed shear and flexural flexibility model with shear-flexure interaction for R/C members subjected to seismic loading," *Earthquake Engineering & Structural Dynamics* **37**(12), 1349–1370.
Mergos, P. E. and Kappos, A. J. [2012] "A gradual spread inelasticity model for R/C beam–columns, accounting for flexure, shear and anchorage slip," *Engineering Structures* **44**, 94–106.
Metelli, G., Messali, F., Beschi, C. and Riva, P. [2015] "A model for beam–column corner joints of existing RC frame subjected to cyclic loading," *Engineering Structures* **89**, 79–92.
Molina, F. J., Verzeletti, G., Magonette, G. E., Buchet, P. and Géradin, M. [1999] "Bi-directional pseudodynamic test of a full-size three-storey building," *Earthquake Engineering & Structural Dynamics* **28**(12), 1541–1566.
Negro, P., Mola, E., Molina, F. J. and Magonette, G. E. [2004] "Full-scale PSD testing of a torsionally unbalanced three-storey non-seismic RC frame," *13th World Conference on Earthquake Engineering*, Vancouver, Canada.
O'Reilly, G. J. [2016] "Performance-Based Seismic Assessment and Retrofit of Existing RC Frame Buildings in Italy," PhD Thesis, IUSS Pavia, Italy.
O'Reilly, G. J. and Sullivan, T. J. [2015] "Influence of modelling parameters on the fragility assessment of pre-1970 Italian RC structures," *COMPDYN 2015-5th ECCOMAS Thematic Conference on Computational Methods in Structural Dynamics and Earthquake Engineering*, Crete Island, Greece.
O'Reilly, G. J. and Sullivan, T. J. [2015b] "Direct displacement-based seismic design of eccentrically braced steel frames," *Journal of Earthquake Engineering* **20**(2), 243–278.

O'Reilly, G. J. and Sullivan, T. J. [2017] "Modelling uncertainty in existing Italian RC frames," *COMPDYN 2017-6th International Conference on Computational Methods in Structural Dynamics and Earthquake Engineering*, Rhodes Island, Greece.

O'Reilly, G. J., Sullivan, T. J. and Filiatrault, A. [2017] "Implications of a more refined damage estimation approach in the assessment of RC frames," *16th World Conference on Earthquake Engineering*, Santiago, Chile.

Pampanin, S., Calvi, G. M. and Moratti, M. [2002] "Seismic behaviour of RC beam-column joints designed for gravity loads," *12th European Conference on Earthquake Engineering*, London, UK.

Pampanin, S., Magenes, G. and Carr, A. J. [2003] "Modelling of shear hinge mechanism in poorly detailed RC beam-column joints," *Concrete Structures in Seismic Regions*, Athens, Greece.

Park, R. and Paulay, T. [1975] *Reinforced Concrete Structures*, John Wiley & Sons, Ltd, New York.

Paulay, T. and Priestley, M. J. N. [1992] *Seismic Design of Reinforced Concrete and Masonry Buildings*, John Wiley & Sons, Ltd, New York.

Priestley, M. J. N. [1997] "Displacement-based seismic assessment of reinforced concrete buildings," *Journal of Earthquake Engineering* **1**(1), 157–192.

Priestley, M. J. N., Calvi, G. M. and Kowalsky, M. J. [2007] *Displacement Based Seismic Design of Structures*, IUSS Press, Pavia, Italy.

Priestley, M. J. N., Seible, F., Verma, R. and Xiao, Y. [1993] "Seismic shear strength of reinforced concrete columns," *Report SSRP-93/06*, San Diego, CA, USA.

Regio Decreto. [1939] Norme perL'esecuzione Delle Opere Conglomerato Cementizio Semplice Od Armato - 2229/39, Rome, Italy.

Ricci, P., De Luca, F. and Verderame, G. M. [2011] "6th April 2009 L'Aquila earthquake, Italy: reinforced concrete building performance," *Bulletin of Earthquake Engineering* **9**(1), 285–305.

Ruggiero, D. M., Bentz, E. C., Calvi, G. M. and Collins, M. P. [2016] "Shear response under reversed cyclic loading," *ACI Structural Journal* **113**(6), 1313–1324.

Salvatore, W., Caprilli, S. and Barberi, V. [2009] *Rapporto Dei Danni Provocati dall'Evento Sismico Del 6 Aprile Sugli Edifici Scolastici Del Centro Storico dell'Aquila*, *Reluis Report* Pisa, Italy. www.reluis.it.

Sassun, K., Sullivan, T. J., Morandi, P. and Cardone, D. [2015] "Characterising the in-plane seismic performance of infill masonry," *Bulletin of the New Zealand Society for Earthquake Engineering* **49**(1), 100–117.

Shafaei, J., Zareian, M. S., Hosseini, A. and Marefat, M. S. [2014] "Effects of joint flexibility on lateral response of reinforced concrete frames," *Engineering Structures* **81**, 412–431.

Sharma, A., Eligehausen, R. and Reddy, G. R. [2011] "A new model to simulate joint shear behavior of poorly detailed beam–column connections in RC structures under seismic loads, Part I: exterior joints," *Engineering Structures* **33**(3), 1034–1051.

Vecchio, F. J. and Collins, M. P. [1986] "The modified compression-field theory for reinforced concrete elements subjected to shear," *ACI Journal Proceedings* **83**(2), 219–231.

Verderame, G. M., Fabbrocino, G. and Manfredi, G. [2008a] "Seismic response of r.c. columns with smooth reinforcement. Part I: monotonic tests," *Engineering Structures* **30**(9), 2277–2288.

Verderame, G. M., Fabbrocino, G. and Manfredi, G. [2008b] "Seismic response of r.c. columns with smooth reinforcement. Part II: cyclic tests," *Engineering Structures* **30**(9), 2289–2300.

Verderame, G. M., Iervolino, I. and Ricci, P. [2009] *Report on the Damage on Buildings Following the Seismic Event of 6th of April 2009 Time 1:32 - L'Aquila M=5.8*.

Verderame, G. M., Polese, M., Mariniello, C. and Manfredi, G. [2010] "A simulated design procedure for the assessment of seismic capacity of existing reinforced concrete buildings," *Advances in Engineering Software* **41**(2), 323–335.

Vona, M. and Masi, A. [2004] "Resistenza sismica de telai in c.a. progettati con il R.D. 2229/39," *XI Congresso Nazionale "L'Ingegneria Sismica in Italia,"* Genova, Italia.

Zimos, D. K., Mergos, P. E. and Kappos, A. J. [2015] "Shear hysteresis model for reinforced concrete elements including the post-peak range," *COMPDYN 2015-5th ECCOMAS Thematic Conference on Computational Methods in Structural Dynamics and Earthquake Engineering*, Crete Island, Greece.